

Pure-mode correlation functions for cosmic shear and application to KiDS-1000

Peter Schneider¹, Marika Asgari², Yasaman Najafi Jozani¹, Andrej Dvornik³, Benjamin Giblin², Joachim Harnois-D'éraps⁴, Catherine Heymans^{2,3}, Hendrik Hildebrandt³, Henk Hoekstra⁵, Konrad Kuijken⁵, Huan Yuan Shan^{6,7}, Tilman Tröster², Angus H. Wright³

¹Argelander-Institut für Astronomie, Universität Bonn, Auf dem Hügel 71, D-53121 Bonn, Germany, e-mail: peter@astro.uni-bonn.de

²Institute for Astronomy, University of Edinburgh, Royal Observatory, Blackford Hill, Edinburgh, EH9 3HJ, U.K.

³Ruhr University Bochum, Faculty of Physics and Astronomy, Astronomical Institute (AIRUB), German Centre for Cosmological Lensing, 44780 Bochum, Germany

⁴School of Mathematics, Statistics and Physics, Newcastle University, Herschel Building, NE1 7RU, Newcastle-upon-Tyne, UK

⁵Leiden Observatory, Leiden University, P.O.Box 9513, 2300RA Leiden, The Netherlands

⁶Shanghai Astronomical Observatory (SHAO), Nandan Road 80, Shanghai 200030, China

⁷University of Chinese Academy of Sciences, Beijing 100049, China

Received ; accepted

ABSTRACT

One probe for systematic effects in gravitational lensing surveys is the presence of so-called B-modes in the cosmic shear two-point correlation functions $\xi_{\pm}(\theta)$, since lensing is expected to produce only E-mode shear. Furthermore, there exist ambiguous modes which can not uniquely be assigned to either E- or B-mode shear. In this paper, we derive explicit equations for the pure-mode shear correlation functions $\xi_{\pm}^{E/B}(\theta)$ and their ambiguous components $\xi_{\pm}^{amb}(\theta)$, that can be derived from the measured $\xi_{\pm}(\theta)$ on a finite angular interval $\theta_{\min} \leq \theta \leq \theta_{\max}$, such that the latter can be decomposed uniquely into pure-mode functions as $\xi_{+} = \xi_{+}^E + \xi_{+}^B + \xi_{+}^{amb}$ and $\xi_{-} = \xi_{-}^E - \xi_{-}^B + \xi_{-}^{amb}$. The derivation is obtained by defining a new set of COSEBIs, for which explicit relations are obtained, and which yields a smaller covariance between COSEBI modes. We derive the relation between $\xi_{\pm}^{E/B/amb}$ and the underlying E-/B-mode power spectra. The pure-mode correlation functions can provide a diagnostics of systematics in configuration space. We then apply our results to SLICS simulations and the KiDS-1000 cosmic shear data, calculate the new COSEBIs and the pure-mode correlation functions, as well as the corresponding covariances, and show that the new statistics fit equally well to the best-fitting cosmological model as the previous KiDS-1000 analysis and recovers the same level of (insignificant) B-modes. We also consider in some detail the ambiguous modes at first- and second-order level, finding some surprising results; for example, the shear field of a point mass, when cut along a line through the center, can not be ascribed uniquely to an E-mode shear and is thus ambiguous, and the shear correlation functions resulting from a random ensemble of point masses, when measured over a finite angular range, correspond to an ambiguous mode.

Key words. cosmology – gravitational lensing – large-scale structure of the Universe

1. Introduction

The statistical analysis of the weak distortions light bundles undergo as they traverse the inhomogeneous Universe (Blandford et al. 1991; Kaiser 1992, 1998) is believed to be the potentially most powerful empirical probe for dark energy (Albrecht et al. 2006; Peacock et al. 2006), provided systematic effects can be controlled to a degree that they are smaller than the statistical error of large weak lensing surveys (see, e.g., Mandelbaum 2018, and references therein). A powerful demonstration of this technique was provided by the CFHTLenS survey (see, e.g., Heymans et al. 2012, 2013; Erben et al. 2013), which revealed that the amplitude of density fluctuations in the low-redshift Universe is smaller than expected from the results obtained by measuring the fluctuations of the cosmic microwave background (CMB). The current generation of ground-based weak lensing surveys – the Kilo Degree Survey (KiDS; e.g., Kuijken et al. 2015, 2019), the Dark Energy Survey (DES, e.g., Drlica-Wagner et al. 2018;

Zuntz et al. 2018), and the Hyper SuprimeCam Survey (HSC; e.g., Aihara et al. 2018) – not only yield impressive improvements over previous surveys in terms of survey area, spectral coverage and/or depth, but also has led to a substantial development of analysis tools, e.g., regarding shear estimates and the determination of the redshift distribution of source galaxies. They also led to a consolidation of the tension regarding the level of density fluctuations as measured by weak lensing and the CMB (Heymans et al. 2021); but also see DES Collaboration et al. (2021) for less discrepant results. For a review on cosmological results from cosmic shear, see Kilbinger (2018).

One of the tests for possible systematics in shear measurements consists in the measurements of B-mode shear (Crittenden et al. 2002; Schneider et al. 2002). Gravitational lensing by the large-scale matter distribution in the Universe is expected to yield some B-mode shear due to lens-lens coupling, however with such a small amplitude that it should remain undetectable even in all-sky surveys (Hilbert et al. 2009; Krause & Hirata 2010). The difference between shear and reduced shear

(Schneider & Seitz 1995) affects the E-mode power spectrum (e.g., White 2005; Shapiro 2009; Deshpande et al. 2020), but to leading order does not yield a B-mode contribution (Schneider et al. 2002). Other potential sources of B-mode shear in data could be due to the clustering of source galaxies (Schneider et al. 2002) or the inhomogeneous depth of wide-field surveys (Vale et al. 2004; Heydenreich et al. 2020), but their amplitude again is expected to be below the detection threshold. The expected level of B-modes from intrinsic alignments (see, e.g., Heymans et al. 2006; Joachimi et al. 2013; Giahi-Saravani & Schäfer 2014; Troxel & Ishak 2015; Joachimi et al. 2015; Hilbert et al. 2017; Blazek et al. 2019, and references therein) is quite model dependent and hence uncertain. The most likely cause for any significant B-modes in shear data is thus the incomplete removal of systematic effects, such as accounting for effects of the point-spread function. For that reason, the significant detection of B-modes in a shear survey is considered a clear sign of remaining systematic effects. Note that the opposite conclusion is not valid: The absence of B-modes does not imply that the data is systematic-free. For example, a constant multiplicative bias would create no B-modes, but affect the E-modes; see also Kitching et al. (2019) for more discussion on this issue.

The most basic second-order shear statistics that can be derived from survey data are the shear two-point correlation functions $\xi_{\pm}(\vartheta)$, since their estimates are unbiased by the presence of gaps in the imaging data. Other second-order shear statistics can be obtained as weighted integrals over $\xi_{\pm}(\vartheta)$. Of those, measures which can separate E-mode shear from B-mode shear are of particular interest. One such measure is the aperture mass dispersion, which was introduced in Schneider et al. (1998) and shown in Schneider et al. (2002) to be obtainable in terms of the shear correlation functions. However, as pointed out by Kilbinger et al. (2006), the calculation of the aperture mass dispersion requires the knowledge of the shear correlation function down to zero separation, which can not be measured, e.g., due to the overlapping images of galaxy pairs. The unavailability of ξ_{\pm} at very small angular scales then yields a bias in the aperture mass statistics and a corresponding mixing of E- and B-modes. This issue was addressed in Schneider & Kilbinger (2007), where the general conditions for E/B-mode separating second-order shear measures that can be obtained from $\xi_{\pm}(\vartheta)$ on a finite interval $0 < \vartheta_{\min} \leq \vartheta \leq \vartheta_{\max} < \infty$ were derived.

Based on this result, a complete orthogonal set of E/B-mode separating integrals (COSEBIs) was defined in Schneider et al. (2010; hereafter SEK). The COSEBIs contain the complete E/B-mode separable second-order shear information obtainable from shear correlation functions on a finite angular interval (see also Becker 2013; Becker & Rozo 2016, for a different approach of decomposing the shear correlation functions into E-mode, B-mode and ambiguous mode statistics). Asgari et al. (2012) studied the performance of COSEBIs on tomographic cosmic shear data, where shear auto- and cross-correlation functions are measured from several source galaxy populations with different redshift distributions. In these papers it was demonstrated that the first few COSEBI components contain essentially all the cosmological information, hence they serve as an efficient data compression method. Furthermore, Asgari & Schneider (2015) developed a further data compression by defining compressed COSEBIs (CCOSEBIs); they showed that even for tomographic cosmic shear data, the cosmologically relevant information is contained in less than $\sim n_p^2/2$ modes, where n_p is the number of cosmological parameters. In addition, COSEBIs are less sensitive to density fluctuations on small spatial scales than the shear correlation functions, for a given ϑ_{\min} , and are therefore less af-

ected by ill-understood baryonic effects in structure evolution (Asgari et al. 2020).

In Asgari et al. (2017), COSEBIs and CCOSEBIs were applied to the CFHTLenS cosmic shear data to probe for the presence of B-mode contributions (see also Asgari et al. 2019; Asgari & Heymans 2019, for applications to other cosmic shear data). Using COSEBIs, Giblin et al. (2021) and Gatti et al. (2021) showed that the most recent data sets from the KiDS survey (KiDS-1000; see Kuijken et al. 2019) and DES (DES-Y3; see Sevilla-Noarbe et al. 2021) show no indications of significant B-mode shear. In addition, Asgari et al. (2021) applied three different second-order shear statistics to the KiDS-1000 shear data (Giblin et al. 2021), all yielding consistent results.

Whereas COSEBIs are extremely useful for extracting all E/B-mode separable second-order information from a cosmic shear survey, the interpretation of individual COSEBI modes is less straightforward. Since they are not localized, neither in angular space nor in Fourier space, a significant detection of B-modes with COSEBIs would be difficult to trace back to a given angular scale (see Asgari et al. 2019, for a thorough discussion on this point) and thus to a possible origin of these B-modes. A different approach for separating modes consists in considering pure-mode shear correlation functions $\xi_{\pm E/B}(\vartheta)$, that were first defined in Crittenden et al. (2002); we will refer to them as CNPT correlation functions hereafter. However, estimating these CNPT correlation functions requires the knowledge of the $\xi_{\pm}(\vartheta)$ for all angular scales. Owing to the lack of such measurements, previous applications of these CNPT correlation functions (see, e.g., Hildebrandt et al. 2017 and references therein) required an extrapolation of ξ_{\pm} to the smallest and largest angular scales, or supplementing their measured values by theoretical predictions.

In this paper, we derive a new set of pure-mode correlation functions that we designate as $\xi_{\pm}^{E/B}(\vartheta)$, which can be calculated from the ξ_{\pm} on a finite angular interval. These pure-mode correlation functions can thus be obtained directly from the data without extrapolation or modelling, and can hence be used to study the angular dependence of any possible B-mode shear.

In order to derive $\xi_{\pm}^{E/B}(\vartheta)$, we reconsider COSEBIs, defining them with a slightly different orthogonality relation than used in SEK. We show in Sect. 2 that for a given interval $\vartheta_{\min} \leq \vartheta \leq \vartheta_{\max}$, the shear correlation functions can be decomposed into E-modes, B-modes, and ambiguous modes (see also Bunn 2011, for a mode decomposition of CMB polarization data). The latter are contributions to the shear correlation functions that can not be uniquely ascribed to either E- or B-modes on a finite separation interval, but can be caused by either of them. In Appendix A, we consider in detail these ambiguous modes, both in terms of the shear field, as well as in terms of shear correlation functions and their relation to the E- and B-mode power spectra. For example, we show several examples of ambiguous shear correlation functions which can be obtained either from an E-mode power spectrum, or a B-mode power spectrum, or a mixture thereof.

In Sect. 3, we define the pure-mode correlation functions and derive closed-form expressions for them in terms of the $\xi_{\pm}(\vartheta)$, discuss their general properties, show that the COSEBIs can be obtained in term of the $\xi_{\pm}^{E/B}$, compare them to the CNPT correlation functions derived by Crittenden et al. (2002), to which they converge in the limit of $\vartheta_{\min} \rightarrow 0$ and $\vartheta_{\max} \rightarrow \infty$, and obtain their relation to the E- and B-mode shear power spectra. We then measure both the new dimensionless COSEBIs and the pure-mode correlation functions for the tomographic data of ~ 1000 square degrees of the Kilo Degree Survey (KiDS-1000,

see Asgari et al. 2021; Heymans et al. 2021) and compare them with the predictions from the best fitting Λ CDM cosmology results of Asgari et al. (2021). We also compare the performance of $\xi_{\pm}^{E/B}$ with the CNPT correlation functions using systematic-induced Scinet Light Cone Simulations (SLICS; Harnois-Déraps et al. 2018) following the methodology in Asgari et al. (2019).

We briefly summarize and discuss our main results in Sect. 5. Furthermore, in Appendix B, we present closed-form expressions for the new set of polynomial weight functions for the COSEBIs satisfying their modified orthonormality relation that we employed in this paper, and we provide an explicit code for calculating weight functions that are polynomial in $\ln \vartheta$, yielding the logarithmic COSEBIs. We find that the correlation matrix of the new COSEBIs has considerably lower off-diagonal elements, implying that the new set of COSEBIs yields less mutual dependence than the previous one. Appendix C explicitly shows that the COSEBIs related to a subinterval of ϑ_{\min} and ϑ_{\max} can be obtained from those on the full interval, and that the ambiguous modes within the subinterval do not depend only on those of the full interval, but also on its COSEBIs, implying that pure-mode information gets transferred to ambiguous modes and thus lost when considering subintervals.

2. E-/B-mode decomposition

2.1. General E-/B-mode decomposition

Throughout this paper, we use the flat-sky approximation; for the largest angular scale considered in practical examples later on (5 degrees), this is expected to be very accurate. We denote by $\xi_{\pm}(\vartheta)$ the two-point correlation functions of shear as a function of angular separation ϑ . It was shown in Schneider & Kilbinger (2007) that an E-/B-mode separation of second-order shear statistics is obtained from the 2PCFs by

$$\begin{aligned} \text{EE} &= \frac{1}{2} \int_0^\infty d\vartheta \vartheta [T_+(\vartheta)\xi_+(\vartheta) + T_-(\vartheta)\xi_-(\vartheta)] , \\ \text{BB} &= \frac{1}{2} \int_0^\infty d\vartheta \vartheta [T_+(\vartheta)\xi_+(\vartheta) - T_-(\vartheta)\xi_-(\vartheta)] , \end{aligned} \quad (1)$$

provided the two weight functions T_{\pm} are related through

$$\int_0^\infty d\vartheta \vartheta J_0(\ell\vartheta)T_+(\vartheta) = \int_0^\infty d\vartheta \vartheta J_4(\ell\vartheta)T_-(\vartheta) \quad (2)$$

or, equivalently,

$$\begin{aligned} T_+(\vartheta) &= T_-(\vartheta) + \int_0^\infty d\theta \theta T_-(\theta) \left(\frac{4}{\vartheta^2} - \frac{12\theta^2}{\vartheta^4} \right) , \\ T_-(\vartheta) &= T_+(\vartheta) + \int_0^\infty d\theta \theta T_+(\theta) \left(\frac{4}{\vartheta^2} - \frac{12\theta^2}{\vartheta^4} \right) , \end{aligned} \quad (3)$$

where J_i are Bessel functions of the first kind. Then, EE and BB contains only E- and B-modes, respectively. Furthermore, Schneider & Kilbinger (2007) showed that an E-/B-mode separation can be obtained from the shear 2PCFs on a finite interval $\vartheta_{\min} \leq \vartheta \leq \vartheta_{\max}$, provided that the function T_+ vanishes outside this interval and satisfies the two conditions

$$\int_{\vartheta_{\min}}^{\vartheta_{\max}} d\vartheta \vartheta T_+(\vartheta) = 0 = \int_{\vartheta_{\min}}^{\vartheta_{\max}} d\vartheta \vartheta^3 T_+(\vartheta) . \quad (4)$$

In this case, the function $T_-(\vartheta)$ as calculated from Eq. (3) also has finite support on the interval $\vartheta_{\min} \leq \vartheta \leq \vartheta_{\max}$, and in addition satisfies the relations

$$\int_{\vartheta_{\min}}^{\vartheta_{\max}} \frac{d\vartheta}{\vartheta} T_-(\vartheta) = 0 = \int_{\vartheta_{\min}}^{\vartheta_{\max}} \frac{d\vartheta}{\vartheta^3} T_-(\vartheta) . \quad (5)$$

The physical reason for the conditions (4), as explained in SEK, is that a constant shear, and a shear field linear in angular position, cannot be uniquely ascribed to either E- or B-modes; these ambiguous modes are therefore filtered out.

2.2. Complete sets of E-/B-modes on a finite interval

In SEK, we constructed two complete orthogonal sets of functions $T_{+n}(\vartheta)$ on the interval $\vartheta_{\min} \leq \vartheta \leq \vartheta_{\max}$, subject to the constraints (4), one of them being polynomials in ϑ , the other being polynomials in $\ln \vartheta$. Here, we consider again complete sets of orthogonal functions on the same interval, however with a slightly different metric. Specifically, we consider a set of functions $T_{+n}(\vartheta)$, $n \geq 1$, which satisfy the orthonormality relation

$$\int_{\vartheta_{\min}}^{\vartheta_{\max}} d\vartheta \vartheta T_{+m}(\vartheta) T_{+n}(\vartheta) = \frac{B}{\bar{\vartheta}^2} \delta_{mn} , \quad (6)$$

for all $m, n \geq 1$, and where each function $T_{+n}(\vartheta)$ satisfies the conditions (4). Here,

$$\bar{\vartheta} = \frac{\vartheta_{\min} + \vartheta_{\max}}{2} , \quad B = \frac{\vartheta_{\max} - \vartheta_{\min}}{\vartheta_{\max} + \vartheta_{\min}} \quad (7)$$

are the mean angular scale within the interval and the relative width, respectively. Note that $\vartheta_{\min} = (1 - B)\bar{\vartheta}$, $\vartheta_{\max} = (1 + B)\bar{\vartheta}$. An explicit construction of such a function set will be given in Appendix B, where we choose $T_{+n}(\vartheta)$ to be a polynomial of order $n + 1$.

For each of the $T_{+n}(\vartheta)$, we define the corresponding function $T_{-n}(\vartheta)$ according to Eq. (3). Interestingly, the T_{-n} also form an orthogonal set of functions on the interval $\vartheta_{\min} \leq \vartheta \leq \vartheta_{\max}$, as we will demonstrate next. For this, we make use of Eq. (2) and the orthogonality relation of Bessel functions to write

$$T_{-n}(\vartheta) = \int_0^\infty d\ell \ell J_4(\ell\vartheta) \int_{\vartheta_{\min}}^{\vartheta_{\max}} d\theta \theta J_0(\ell\theta) T_{+n}(\theta) . \quad (8)$$

Carrying out the ℓ -integration leads to the second of Eqs. (3), but for the present purpose, it is more convenient to keep this presentation. We will now show a convenient property:

Lemma: Consider two functions $F_+(\vartheta)$ and $F'_+(\vartheta)$, defined for $\vartheta \geq 0$, and let $F_-(\vartheta)$ and $F'_-(\vartheta)$ be the functions obtained from them by applying the transformation

$$F_-(\vartheta) = \int_0^\infty d\ell \ell J_4(\ell\vartheta) \int_0^\infty d\theta \theta J_0(\ell\theta) F_+(\theta) . \quad (9)$$

Then,

$$\int_0^\infty d\vartheta \vartheta F_-(\vartheta) F'_-(\vartheta) = \int_0^\infty d\vartheta \vartheta F_+(\vartheta) F'_+(\vartheta) . \quad (10)$$

The proof of the Lemma is rather straightforward: using the transformation (9), we obtain

$$\begin{aligned} \int_0^\infty d\vartheta \vartheta F_-(\vartheta) F'_-(\vartheta) &= \int_0^\infty d\vartheta \vartheta \int_0^\infty d\ell \ell J_4(\ell\vartheta) \\ &\times \int_0^\infty d\theta \theta J_0(\ell\theta) F_+(\theta) \int_0^\infty d\ell' \ell' J_4(\ell'\vartheta) \\ &\times \int_0^\infty d\theta' \theta' J_0(\ell'\theta') F'_+(\theta') . \end{aligned} \quad (11)$$

We now carry out the ϑ -integration, using

$$\int_0^\infty d\vartheta \vartheta J_n(\ell\vartheta) J_n(\ell'\vartheta) = \frac{1}{\ell} \delta_D(\ell - \ell') , \quad (12)$$

after which the ℓ' -integration becomes trivial, yielding

$$\begin{aligned} \int_0^\infty d\vartheta \vartheta F_-(\vartheta) F'_-(\vartheta) &= \int_0^\infty d\ell \ell \int_{\vartheta_{\min}}^{\vartheta_{\max}} d\vartheta \vartheta J_0(\ell\vartheta) F_+(\vartheta) \\ &\times \int_0^\infty d\vartheta' \vartheta' J_0(\ell\vartheta') F'_+(\vartheta') = \int_0^\infty d\vartheta \vartheta F_+(\vartheta) F'_+(\vartheta), \end{aligned} \quad (13)$$

where we applied Eq. (12) again. This completes the proof.

We now apply the Lemma by letting $F_+ = T_{+m}$, $F'_+ = T_{+n}$; noting that the T_{+n} are zero outside the interval $\vartheta_{\min} \leq \vartheta \leq \vartheta_{\max}$, we see from Eqs. (8) and (9) that $F_- = T_{-m}$, $F'_- = T_{-n}$. Therefore,

$$\int_{\vartheta_{\min}}^{\vartheta_{\max}} d\vartheta \vartheta T_{-m}(\vartheta) T_{-n}(\vartheta) = \int_{\vartheta_{\min}}^{\vartheta_{\max}} d\vartheta \vartheta T_{+m}(\vartheta) T_{+n}(\vartheta) = \frac{B}{\bar{\vartheta}^2} \delta_{mn} \quad (14)$$

Thus, the set of $T_{-n}(\vartheta)$ functions obey the same orthogonality relations as the T_{+n} .

In order to obtain a complete set of functions on the interval $\vartheta_{\min} \leq \vartheta \leq \vartheta_{\max}$ irrespective of the conditions (4), we need to augment the set of the T_{+n} by two more functions that do not obey the conditions (4), which we call $T_{+a}(\vartheta)$ and $T_{+b}(\vartheta)$. We choose them as

$$T_{+a}(\vartheta) = \frac{1}{\sqrt{2}\bar{\vartheta}^2}; \quad T_{+b}(\vartheta) = \frac{\sqrt{3}}{2\sqrt{2}B\bar{\vartheta}^2} \left[\left(\frac{\vartheta}{\bar{\vartheta}} \right)^2 - (1 + B^2) \right]. \quad (15)$$

Both functions are normalized according to Eq.(6), and they are mutually orthogonal. Furthermore, both of them are orthogonal to all $T_{+n}(\vartheta)$ due to the conditions (4). Thus, the set of functions $T_{+\mu}(\vartheta)$, $\mu = a, b, 1, 2, \dots$, form a complete orthonormal set of functions on the interval $\vartheta_{\min} \leq \vartheta \leq \vartheta_{\max}$.

We cannot use these two functions in Eq. (3) to obtain corresponding functions $T_{-a,b}$, since those would not have finite support. Instead, we choose the two additional functions

$$\begin{aligned} T_{-a}(\vartheta) &= \frac{1 - B^2}{\sqrt{2}\bar{\vartheta}^2}; \\ T_{-b}(\vartheta) &= \sqrt{\frac{3}{8}} \frac{1 - B^2}{B} \left[\frac{1 + B^2}{\vartheta^2} - \frac{(1 - B^2)^2 \bar{\vartheta}^2}{\vartheta^4} \right], \end{aligned} \quad (16)$$

which are orthogonal to all T_{-n} , according to Eq. (5), and obey the orthonormality relation (14). Thus, we now have two complete orthonormal sets of functions on the interval $\vartheta_{\min} \leq \vartheta \leq \vartheta_{\max}$, the $T_{+\mu}$, and the $T_{-\mu}$.

We now define the quantities E_μ and B_μ through

$$\begin{aligned} E_\mu &= \frac{1}{2} \int_{\vartheta_{\min}}^{\vartheta_{\max}} d\vartheta \vartheta \left[T_{+\mu}(\vartheta) \xi_+(\vartheta) + T_{-\mu}(\vartheta) \xi_-(\vartheta) \right], \\ B_\mu &= \frac{1}{2} \int_{\vartheta_{\min}}^{\vartheta_{\max}} d\vartheta \vartheta \left[T_{+\mu}(\vartheta) \xi_+(\vartheta) - T_{-\mu}(\vartheta) \xi_-(\vartheta) \right]. \end{aligned} \quad (17)$$

For $\mu = n$, with $n \geq 1$, these form the COSEBIs for the given set of functions $T_{\pm n}$, such that E_n depends only on E-mode shear, and B_n contains only B-mode shear. For $\mu = a, b$, E_μ and B_μ do not have an analogous interpretation. Note that the orthonormality condition for the $T_{n\pm}$ used in this paper makes the COSEBIs dimensionless, in contrast to those defined in SEK.

Since the $T_{+\mu}$ and the $T_{-\mu}$ both form a complete orthonormal set of functions, we can write the shear correlation functions on the interval $\vartheta_{\min} \leq \vartheta \leq \vartheta_{\max}$ as a superposition,

$$\xi_\pm(\vartheta) = \frac{\bar{\vartheta}^2}{B} \sum_\mu \tau_{\pm\mu} T_{\pm\mu}(\vartheta); \quad (18)$$

Taking the sum of Eqs. (17), we find

$$\begin{aligned} E_\mu + B_\mu &= \int_{\vartheta_{\min}}^{\vartheta_{\max}} d\vartheta \vartheta T_{+\mu}(\vartheta) \xi_+(\vartheta) \\ &= \frac{\bar{\vartheta}^2}{B} \sum_\nu \tau_{+\nu} \int_{\vartheta_{\min}}^{\vartheta_{\max}} d\vartheta \vartheta T_{+\mu}(\vartheta) T_{+\nu}(\vartheta) = \tau_{+\mu}, \end{aligned} \quad (19)$$

where we inserted the expansion (18) and made use of the orthogonality relation (6). From the difference of Eqs. (17), we obtain in complete analogy

$$E_\mu - B_\mu = \int_{\vartheta_{\min}}^{\vartheta_{\max}} d\vartheta \vartheta T_{-\mu}(\vartheta) \xi_-(\vartheta) = \tau_{-\mu}, \quad (20)$$

so that

$$E_\mu = \frac{\tau_{+\mu} + \tau_{-\mu}}{2}; \quad B_\mu = \frac{\tau_{+\mu} - \tau_{-\mu}}{2}. \quad (21)$$

3. Pure-mode correlation functions

In this section, we will consider the pure-mode correlation functions; more specifically, we will show that the shear correlation functions can be decomposed as

$$\begin{aligned} \xi_+(\vartheta) &= \xi_+^E(\vartheta) + \xi_+^B(\vartheta) + \xi_+^{\text{amb}}(\vartheta); \\ \xi_-(\vartheta) &= \xi_-^E(\vartheta) - \xi_-^B(\vartheta) + \xi_-^{\text{amb}}(\vartheta), \end{aligned} \quad (22)$$

where the pure E- and B-mode correlation functions are defined in terms of the COSEBIs,

$$\xi_+^E(\vartheta) := \frac{\bar{\vartheta}^2}{B} \sum_{n=1}^\infty E_n T_{+n}(\vartheta); \quad \xi_+^B(\vartheta) := \frac{\bar{\vartheta}^2}{B} \sum_{n=1}^\infty B_n T_{+n}(\vartheta), \quad (23)$$

$$\xi_-^E(\vartheta) := \frac{\bar{\vartheta}^2}{B} \sum_{n=1}^\infty E_n T_{-n}(\vartheta); \quad \xi_-^B(\vartheta) := \frac{\bar{\vartheta}^2}{B} \sum_{n=1}^\infty B_n T_{-n}(\vartheta), \quad (24)$$

and the ξ_\pm^{amb} correspond to ambiguous modes. In Sect. 3.1, we consider general properties of these pure-mode correlation functions. We express these as integrals over the ξ_\pm in Sect. 3.2; hence, in order to calculate the pure-mode correlation functions, one does not need to calculate the COSEBIs as intermediate step. Readers less interested in the derivation of the results can find the final expressions for the pure-mode correlation function in Eqs. (41, 42, 53, 54). In Sect. 3.3, we compare our pure-mode correlation functions to the CNPT correlation functions that were defined previously in Crittenden et al. (2002) and Schneider et al. (2002), but not confined to a finite separation interval. Some consistency checks for the pure-mode correlation functions are described in Sect. 3.4, and their relation to the power spectra is derived in Sect. 3.5.

3.1. General properties

According to these definitions and the constraints (4) and (5) that the basis functions $T_{\pm n}$ have to satisfy, we find that

$$\int_{\vartheta_{\min}}^{\vartheta_{\max}} d\vartheta \vartheta \xi_{+}^{\text{E,B}}(\vartheta) = 0 = \int_{\vartheta_{\min}}^{\vartheta_{\max}} d\vartheta \vartheta^3 \xi_{+}^{\text{E,B}}(\vartheta); \quad (25)$$

$$\int_{\vartheta_{\min}}^{\vartheta_{\max}} \frac{d\vartheta}{\vartheta} \xi_{-}^{\text{E,B}}(\vartheta) = 0 = \int_{\vartheta_{\min}}^{\vartheta_{\max}} \frac{d\vartheta}{\vartheta^3} \xi_{-}^{\text{E,B}}(\vartheta). \quad (26)$$

These relations show that the pure-mode correlation functions need to have (at least) two roots in the interval $\vartheta_{\min} \leq \vartheta \leq \vartheta_{\max}$, and hence their functional form can be expected to differ substantially from $\xi_{\pm}(\vartheta)$. An example for this was shown in Fig. 7 of SEK, where an equivalent definition of the pure-mode correlation functions was applied. Furthermore, since $T_{-n}(\vartheta_{\min}) = T_{+n}(\vartheta_{\min})$ and $T_{-n}(\vartheta_{\max}) = T_{+n}(\vartheta_{\max})$, we find that

$$\xi_{+}^{\text{E/B}}(\vartheta_{\min}) = \xi_{-}^{\text{E/B}}(\vartheta_{\min}), \quad \xi_{+}^{\text{E/B}}(\vartheta_{\max}) = \xi_{-}^{\text{E/B}}(\vartheta_{\max}). \quad (27)$$

As expected, the COSEBIs can be expressed in terms of the pure-mode correlation functions, as we find from Eqs. (23, 24) by multiplying them with $\vartheta T_{\pm m}(\vartheta)$ and integrating over ϑ , making use of the orthogonality relation (14):

$$\begin{aligned} \int_{\vartheta_{\min}}^{\vartheta_{\max}} d\vartheta \vartheta \xi_{+}^{\text{E}}(\vartheta) T_{+m}(\vartheta) &= E_m = \int_{\vartheta_{\min}}^{\vartheta_{\max}} d\vartheta \vartheta \xi_{-}^{\text{E}}(\vartheta) T_{-m}(\vartheta); \\ \int_{\vartheta_{\min}}^{\vartheta_{\max}} d\vartheta \vartheta \xi_{+}^{\text{B}}(\vartheta) T_{+m}(\vartheta) &= B_m = \int_{\vartheta_{\min}}^{\vartheta_{\max}} d\vartheta \vartheta \xi_{-}^{\text{B}}(\vartheta) T_{-m}(\vartheta). \end{aligned} \quad (28)$$

The foregoing equations allow us to find relations between $\xi_{+}^{\text{E/B}}(\vartheta)$ and $\xi_{-}^{\text{E/B}}(\vartheta)$. We start with a consistency relation, by using the definition (23) and replacing E_n or B_n by the first expression in (28), which yields

$$\begin{aligned} \xi_{+}^{\text{E/B}}(\vartheta) &= \frac{\bar{\vartheta}^2}{B} \sum_{n=1}^{\infty} T_{+n}(\vartheta) \int d\theta \theta \xi_{+}^{\text{E/B}}(\theta) T_{+n}(\theta) \\ &= \frac{\bar{\vartheta}^2}{B} \sum_{\mu} T_{+\mu}(\vartheta) \int d\theta \theta \xi_{+}^{\text{E/B}}(\theta) T_{+\mu}(\theta) = \xi_{+}^{\text{E/B}}(\vartheta), \end{aligned} \quad (29)$$

where in the second step we made use of the fact that $\xi_{+}^{\text{E/B}}$ is orthogonal to T_{+a} and T_{+b} , so that we could extend the sum over all $\mu = a, b, 1, 2, \dots$. In the final step, we made use of the completeness of the $T_{+\mu}$, which implies

$$\frac{\bar{\vartheta}^2}{B} \sum_{\mu} T_{+\mu}(\vartheta) T_{+\mu}(\theta) = \frac{1}{\theta} \delta_{\text{D}}(\vartheta - \theta). \quad (30)$$

Next we derive a relation between $\xi_{+}^{\text{E/B}}$ and $\xi_{-}^{\text{E/B}}$, again using Eqs. (23) and (28),

$$\xi_{+}^{\text{E/B}}(\vartheta) = \frac{\bar{\vartheta}^2}{B} \sum_{n=1}^{\infty} T_{+n}(\vartheta) \int d\theta \theta \xi_{-}^{\text{E/B}}(\theta) T_{-n}(\theta). \quad (31)$$

We consider the sum

$$\begin{aligned} &\sum_{n=1}^{\infty} T_{+n}(\vartheta) T_{-n}(\theta) \\ &= \sum_{n=1}^{\infty} T_{+n}(\vartheta) \left[T_{+n}(\theta) + \int_{\vartheta_{\min}}^{\theta} d\varphi \varphi T_{+n}(\varphi) \left(\frac{4}{\theta^2} - \frac{12\varphi^2}{\theta^4} \right) \right] \\ &= \sum_{\mu} T_{+\mu}(\vartheta) \left[T_{+\mu}(\theta) + \int_{\vartheta_{\min}}^{\theta} d\varphi \varphi T_{+\mu}(\varphi) \left(\frac{4}{\theta^2} - \frac{12\varphi^2}{\theta^4} \right) \right] \\ &\quad - \sum_{\mu=a,b} T_{+\mu}(\vartheta) \left[T_{+\mu}(\theta) + \int_{\vartheta_{\min}}^{\theta} d\varphi \varphi T_{+\mu}(\varphi) \left(\frac{4}{\theta^2} - \frac{12\varphi^2}{\theta^4} \right) \right]. \end{aligned}$$

The sum over all μ can be carried out using the completeness relation (30). For the sum over $\mu = a, b$, we can calculate the term in the bracket, to find that for $\mu = a$ and $\mu = b$, the result is of the form $a/\theta^2 + b/\theta^4$, and hence can be expressed in terms of the $T_{-a,b}(\theta)$. Thus we find that

$$\begin{aligned} &\frac{\bar{\vartheta}^2}{B} \sum_{n=1}^{\infty} T_{+n}(\vartheta) T_{-n}(\theta) \\ &= \frac{\delta_{\text{D}}(\vartheta - \theta)}{\vartheta} + H(\vartheta - \theta) \left(\frac{4}{\theta^2} - \frac{12\vartheta^2}{\theta^4} \right) \\ &\quad - X_a(\vartheta) T_{-a}(\theta) - X_b(\vartheta) T_{-b}(\theta), \end{aligned} \quad (32)$$

where the $X_{a,b}(\vartheta)$ are quadratic functions of ϑ whose actual form is of no relevance here. Inserting this result into Eq. (31), and making use of the fact that $\xi_{-}^{\text{E/B}}$ is orthogonal to T_{-a} and T_{-b} , we finally find

$$\xi_{+}^{\text{E/B}}(\vartheta) = \xi_{-}^{\text{E/B}}(\vartheta) + \int_{\vartheta}^{\vartheta_{\max}} d\theta \theta \xi_{-}^{\text{E/B}}(\theta) \left(\frac{4}{\theta^2} - \frac{12\vartheta^2}{\theta^4} \right). \quad (33)$$

Thus we obtain a relation between $\xi_{+}^{\text{E/B}}$ and $\xi_{-}^{\text{E/B}}$ that is very similar to the one between ξ_{+} and ξ_{-} in the absence of B-modes,

$$\xi_{+}(\vartheta) = \xi_{-}(\vartheta) + \int_{\vartheta}^{\infty} d\theta \theta \xi_{-}(\theta) \left(\frac{4}{\theta^2} - \frac{12\vartheta^2}{\theta^4} \right), \quad (34)$$

except that the integral only extends to ϑ_{\max} . We can see from Eq. (33) that the conditions (27) are satisfied; for $\vartheta = \vartheta_{\max}$ this is trivial, and for $\vartheta = \vartheta_{\min}$, it follows from the functional form of the integrand and the orthogonality of $\xi_{-}^{\text{E/B}}$ to the $T_{-a,b}$.

Using analogous steps, one can derive the inverse of the relation,

$$\begin{aligned} \xi_{-}^{\text{E/B}}(\vartheta) &= \frac{\bar{\vartheta}^2}{B} \sum_{n=1}^{\infty} E_n T_{-n}(\vartheta) \\ &= \xi_{+}^{\text{E/B}}(\vartheta) + \int_{\vartheta_{\min}}^{\vartheta} d\theta \theta \xi_{+}^{\text{E/B}}(\theta) \left(\frac{4}{\theta^2} - \frac{12\vartheta^2}{\theta^4} \right), \end{aligned} \quad (35)$$

again in close analogy to a corresponding relation between ξ_{+} and ξ_{-} in the absence of B-modes.

We would like to point out that the pure-mode correlation functions $\xi_{+}^{\text{E/B}}(\vartheta)$, $\xi_{-}^{\text{E/B}}(\vartheta)$, and the set of COSEBIs E_n and B_n , respectively, contain exactly the same information, as Eqs. (33, 35, 23, 24) show that one of these quantities can be derived from any of the other two. In practice, this exact equivalence will apply only approximately, due to the finite number of COSEBI modes and the finite binning of the correlation functions; we shall demonstrate this issue in Sect. 4 below.

3.2. Pure-mode correlation functions from ξ_{\pm}

Obviously, we can calculate these pure-mode correlation functions from the set of the E_n , B_n that can be calculated from Eqs. (17). However, as we will show here, they can also be obtained without first calculating the (infinite) set of COSEBIs. For that, we consider

$$\begin{aligned}\xi_+^E(\vartheta) + \xi_+^B(\vartheta) &= \frac{\bar{\vartheta}^2}{B} \left(\sum_{\mu} \tau_{+\mu} T_{+\mu}(\vartheta) - \tau_{+a} T_{+a}(\vartheta) - \tau_{+b} T_{+b}(\vartheta) \right) \\ &= \xi_+(\vartheta) - [\tau_{+a} U_{+a}(\vartheta) + \tau_{+b} U_{+b}(\vartheta)] ,\end{aligned}\quad (36)$$

where we made use of Eq. (18), and defined for $\mu = a, b$,

$$U_{+\mu}(\vartheta) = \frac{\bar{\vartheta}^2}{B} T_{+\mu}(\vartheta) . \quad (37)$$

Thus, in order to calculate this sum, we only need the two coefficients $\tau_{+a,b}$ that can be calculated from ξ_+ using Eq. (19). Similarly,

$$\begin{aligned}\xi_+^E(\vartheta) - \xi_+^B(\vartheta) &= \frac{\bar{\vartheta}^2}{B} \sum_{n=1}^{\infty} \tau_{-n} T_{-n}(\vartheta) \\ &= \frac{\bar{\vartheta}^2}{B} \sum_{n=1}^{\infty} \tau_{-n} \left[T_{-n}(\vartheta) + \int_{\vartheta}^{\vartheta_{\max}} \frac{d\theta}{\theta} T_{-n}(\theta) \left(4 - \frac{12\vartheta^2}{\theta^2} \right) \right] \\ &= \xi_-(\vartheta) + \int_{\vartheta}^{\vartheta_{\max}} \frac{d\theta}{\theta} \xi_-(\theta) \left(4 - \frac{12\vartheta^2}{\theta^2} \right) \\ &\quad - \frac{\bar{\vartheta}^2}{B} \sum_{\mu=a,b} \tau_{-\mu} \left[T_{-\mu}(\vartheta) + \int_{\vartheta}^{\vartheta_{\max}} \frac{d\theta}{\theta} T_{-\mu}(\theta) \left(4 - \frac{12\vartheta^2}{\theta^2} \right) \right] ,\end{aligned}\quad (38)$$

where we used the relation (3) between the T_{+n} and T_{-n} and the decomposition (18). The expression in the final bracket of Eq. (38) can be calculated, using Eq. (16). For both $\mu = a, b$, the resulting expressions are of the form $a + b\vartheta^2$, and thus can be written in terms of the $U_{+\mu}$. We then find

$$\begin{aligned}\xi_+^E(\vartheta) - \xi_+^B(\vartheta) &= \xi_-(\vartheta) + \int_{\vartheta}^{\vartheta_{\max}} \frac{d\theta}{\theta} \xi_-(\theta) \left(4 - \frac{12\vartheta^2}{\theta^2} \right) \\ &\quad - \sum_{\mu=a,b} \tau_{-\mu} U_{-\mu}(\vartheta) ,\end{aligned}\quad (39)$$

where

$$\begin{aligned}U_{-a}(\vartheta) &= \frac{1-B}{\sqrt{2}B(1+B)^3} \left[3 \left(\frac{\vartheta}{\bar{\vartheta}} \right)^2 - 2(1+B)^2 \right] , \\ U_{-b}(\vartheta) &= \frac{\sqrt{3}}{\sqrt{8}B^2} \left[\frac{(1-B)(1+4B+B^2)}{(1+B)^3} \left(\frac{\vartheta}{\bar{\vartheta}} \right)^2 - (1-B^2) \right] .\end{aligned}\quad (40)$$

We then finally obtain for the pure mode correlation functions

$$\begin{aligned}\xi_+^E(\vartheta) &= \frac{1}{2} \left[\xi_+(\vartheta) + \xi_-(\vartheta) + \int_{\vartheta}^{\vartheta_{\max}} \frac{d\theta}{\theta} \xi_-(\theta) \left(4 - \frac{12\vartheta^2}{\theta^2} \right) \right] \\ &\quad - \frac{1}{2} [S_+(\vartheta) + S_-(\vartheta)] ;\end{aligned}\quad (41)$$

$$\begin{aligned}\xi_+^B(\vartheta) &= \frac{1}{2} \left[\xi_+(\vartheta) - \xi_-(\vartheta) - \int_{\vartheta}^{\vartheta_{\max}} \frac{d\theta}{\theta} \xi_-(\theta) \left(4 - \frac{12\vartheta^2}{\theta^2} \right) \right] \\ &\quad - \frac{1}{2} [S_+(\vartheta) - S_-(\vartheta)] .\end{aligned}\quad (42)$$

Here, we have defined

$$S_+(\vartheta) \equiv \sum_{\mu=a,b} \tau_{+\mu} U_{+\mu}(\vartheta) = \int_{\vartheta_{\min}}^{\vartheta_{\max}} \frac{d\theta}{\bar{\vartheta}^2} \xi_+(\theta) H_+(\vartheta, \theta) ; \quad (43)$$

$$S_-(\vartheta) \equiv \sum_{\mu=a,b} \tau_{-\mu} U_{-\mu}(\vartheta) = \int_{\vartheta_{\min}}^{\vartheta_{\max}} \frac{d\theta}{\theta} \xi_-(\theta) H_-(\vartheta, \theta) , \quad (44)$$

where

$$\begin{aligned}H_+(\vartheta, \theta) &= \bar{\vartheta}^2 \sum_{\mu=a,b} T_{+\mu}(\theta) U_{+\mu}(\vartheta) \\ &= \frac{1}{8B^3} \left\{ 4B^2 + 3 \left[\left(\frac{\vartheta}{\bar{\vartheta}} \right)^2 - 1 - B^2 \right] \left[\left(\frac{\theta}{\bar{\vartheta}} \right)^2 - 1 - B^2 \right] \right\} ;\end{aligned}\quad (45)$$

$$\begin{aligned}H_-(\vartheta, \theta) &= \theta^2 \sum_{\mu=a,b} T_{-\mu}(\theta) U_{-\mu}(\vartheta) \\ &= \frac{(1-B)^2}{8B^3} \left\{ 3(1-B)^2 \left[(1+B)^4 - (1+4B+B^2) \left(\frac{\vartheta}{\bar{\vartheta}} \right)^2 \right] \left(\frac{\theta}{\bar{\vartheta}} \right)^{-2} \right. \\ &\quad \left. + \left[3(1+B)^2 \left(\frac{\vartheta}{\bar{\vartheta}} \right)^2 - (3+6B+14B^2+6B^3+3B^4) \right] \right\} ,\end{aligned}\quad (46)$$

and where we made use of Eq. (19) and the forgoing expressions for the $U_{\pm\mu}$. We note that the functions $S_{\pm}(\vartheta)$ are of the form $a + b\vartheta^2$, and thus correspond to a shear correlation caused by ambiguous modes. Indeed, by adding the two Eqs. (41) and (42), we obtain the first of Eq. (22), with $\xi_+^{\text{amb}}(\vartheta) = S_+(\vartheta)$. It is important to realize that the final expressions for $S_{\pm}(\vartheta)$ are independent of the specific choice of the functions $T_{\pm a,b}$. It is easy to see that any ‘rotation’ in the two-dimensional subspace of functions which do not obey the conditions (4) or (5), respectively, leaves the forgoing expressions invariant.

We plot an example for the decomposition of the shear correlation function ξ_+ into E-modes and ambiguous modes in the upper panel of Fig. 1. For separations close to ϑ_{\min} , $\xi_+^E(\vartheta)$ is close to $\xi_+(\vartheta)$; however, for larger values of ϑ , these two functions are markedly different, due to the increasing amplitude of the ambiguous modes. As expected, $\xi_+^E(\vartheta)$ has two roots in the interval considered, whereas $\xi_+(\vartheta)$ stays positive.

At first sight, one might wonder that the ambiguous correlation function has a large amplitude. But what should be kept in mind is that the information of this function is contained solely in two numbers. In particular, as was shown in Asgari et al. (2012), they contain little cosmological information even if assumed to be solely due to E-mode shear.

Next, we turn to the ‘-’ pure mode correlation functions. Using in turn Eqs. (24), (18), (3), and (43), we find

$$\begin{aligned}\xi_-^E(\vartheta) + \xi_-^B(\vartheta) &= \frac{\bar{\vartheta}^2}{B} \sum_{n=1}^{\infty} \tau_{+n} T_{-n}(\vartheta) \\ &= \frac{\bar{\vartheta}^2}{B} \sum_{n=1}^{\infty} \tau_{+n} \left[T_{+n}(\vartheta) + \int_{\vartheta_{\min}}^{\vartheta} \frac{d\theta}{\theta} T_{+n}(\theta) \left(4 - \frac{12\vartheta^2}{\theta^2} \right) \right] \\ &= \xi_+(\vartheta) - S_+(\vartheta) + \int_{\vartheta_{\min}}^{\vartheta} \frac{d\theta}{\theta} \xi_+(\theta) [S_+(\vartheta) - S_+(\theta)] \left(4 - \frac{12\vartheta^2}{\theta^2} \right) \\ &= \xi_+(\vartheta) + \int_{\vartheta_{\min}}^{\vartheta} \frac{d\theta}{\theta} \xi_+(\theta) \left(4 - \frac{12\vartheta^2}{\theta^2} \right) - V_+(\vartheta) ,\end{aligned}\quad (47)$$

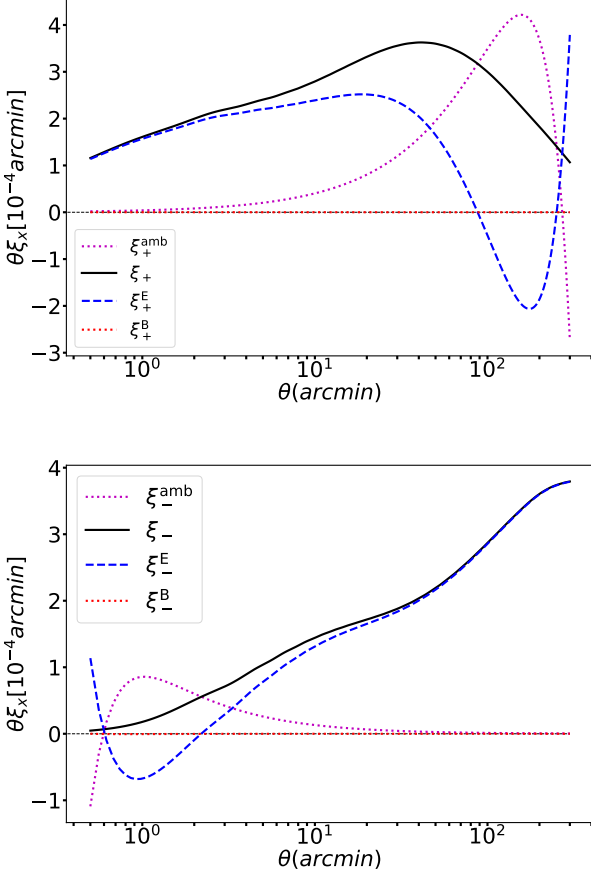


Fig. 1. Decomposition of the shear correlation functions $\xi_+(\theta)$ (upper panel) and $\xi_-(\theta)$ (lower panel) into pure E-modes (dashed blue curves) and ambiguous modes (dotted magenta curves). The latter are quadratic functions of θ and $1/\theta$ for ξ_+ and ξ_- , respectively. Note that $\xi_+ = \xi_+^E + \xi_+^{\text{amb}}$, due to the absence of B-mode shear assumed for this plot. Here, we chose $\vartheta_{\min} = 0.5'$ and $\vartheta_{\max} = 300'$, and the correlation function ξ_{\pm} were calculated for a standard cosmological model fitted to the KiDS-1000 cosmic shear data (see Table 1). The source redshift distribution corresponds to the highest tomographic bin of KiDS-1000 data.

Table 1. Fiducial cosmological parameters.

S_8	Ω_m	Ω_b	h	n_s	A_{IA}	A_{bary}
0.759	0.246	0.015	0.767	0.901	0.264	2.859

Notes. We employ a flat Λ CDM model with parameters fitted to the KiDS-1000 cosmic shear data (Asgari et al. 2021). The structure growth parameter, $S_8 = \sigma_8(\Omega_m/0.3)^{0.5}$, and the amplitude of the intrinsic alignments of galaxies, A_{IA} , are the only two parameters that KiDS-1000 cosmic shear data constrains. Ω_m is the total matter density parameter and Ω_b represents the density parameter for baryonic matter. The spectral index of the primordial power spectrum is denoted as n_s , while h represents the dimensionless Hubble parameter. We allow for baryonic feedback through A_{bary} , which is equal to 3.13 for a dark matter only scenario. Additionally, the sum of the neutrino masses is fixed to 0.06 eV.

where we have defined the function

$$V_+(\vartheta) = S_+(\vartheta) + \int_{\vartheta_{\min}}^{\vartheta} \frac{d\theta}{\theta^2} S_+(\theta) \left(4 - \frac{12\theta^2}{\vartheta^2}\right) = \int_{\vartheta_{\min}}^{\vartheta_{\max}} \frac{d\theta}{\theta^2} \xi_+(\theta) K_+(\vartheta, \theta), \quad (48)$$

and by using the definition (43) for S_+ , we obtain for the kernel K_+ the following expression:

$$K_+(\vartheta, \theta) = H_+(\vartheta, \theta) + \int_{\vartheta_{\min}}^{\vartheta} \frac{d\varphi}{\varphi^2} H_+(\varphi, \theta) \left(4 - \frac{12\varphi^2}{\vartheta^2}\right) = \frac{(1-B)^2}{8B^3} \left\{ 3(1-B)^2 \left(\frac{\vartheta}{\theta}\right)^{-4} \left[(1+B)^4 - (1+4B+B^2) \left(\frac{\theta}{\vartheta}\right)^2 \right] + \left(\frac{\vartheta}{\theta}\right)^{-2} \left[3(1+B)^2 \left(\frac{\theta}{\vartheta}\right)^2 - (3+6B+14B^2+6B^3+3B^4) \right] \right\} = \left(\frac{\vartheta}{\theta}\right)^2 H_-(\theta, \vartheta). \quad (49)$$

For the difference of the two ‘-’ correlation functions we obtain

$$\xi_-^E(\vartheta) - \xi_-^B(\vartheta) = \frac{\bar{\vartheta}^2}{B} \sum_{n=1}^{\infty} \tau_{-n} T_{-n}(\vartheta) = \xi_-^E(\vartheta) - V_-(\vartheta), \quad (50)$$

where

$$V_-(\vartheta) = \frac{\bar{\vartheta}^2}{B} \sum_{\mu=a,b} \tau_{-\mu} T_{-\mu}(\vartheta) = \int_{\vartheta_{\min}}^{\vartheta_{\max}} \frac{d\theta}{\theta^2} \xi_-(\theta) K_-(\vartheta, \theta), \quad (51)$$

with the kernel function

$$K_-(\vartheta, \theta) = \frac{\bar{\vartheta}^4}{B} \sum_{\mu=a,b} T_{-\mu}(\vartheta) T_{-\mu}(\theta) = \frac{\bar{\vartheta}^4(1-B^2)^2}{B\vartheta^2\theta^2} \left\{ \frac{1}{2} + \frac{3}{8B^2} \left[1+B^2 - (1-B^2)^2 \left(\frac{\bar{\vartheta}}{\theta}\right)^2 \right] \times \left[1+B^2 - (1-B^2)^2 \left(\frac{\bar{\vartheta}}{\theta}\right)^2 \right] \right\} = \frac{(1-B^2)^2\bar{\vartheta}^4}{\vartheta^2\theta^2} H_+ \left(\frac{[1-B^2]\bar{\vartheta}^2}{\theta}, \frac{[1-B^2]\bar{\vartheta}^2}{\theta} \right). \quad (52)$$

Therefore,

$$\xi_-^E(\vartheta) = \frac{1}{2} \left[\xi_+(\vartheta) + \xi_-(\vartheta) + \int_{\vartheta_{\min}}^{\vartheta} \frac{d\theta}{\theta^2} \xi_+(\theta) \left(4 - \frac{12\theta^2}{\vartheta^2}\right) \right] - \frac{1}{2} [V_+(\vartheta) + V_-(\vartheta)], \quad (53)$$

$$\xi_-^B(\vartheta) = \frac{1}{2} \left[\xi_+(\vartheta) - \xi_-(\vartheta) + \int_{\vartheta_{\min}}^{\vartheta} \frac{d\theta}{\theta^2} \xi_+(\theta) \left(4 - \frac{12\theta^2}{\vartheta^2}\right) \right] - \frac{1}{2} [V_+(\vartheta) - V_-(\vartheta)]. \quad (54)$$

The functions $V_{\pm}(\vartheta)$ are of the form $a\vartheta^{-2} + b\vartheta^{-4}$, and therefore correspond to shear correlations due to ambiguous modes. These are subtracted from the rest of the expression to yield pure E- and B-mode correlation functions. By subtracting Eq. (54) from Eq. (53), we obtain the second of Eqs. 22, with $\xi_-^{\text{amb}}(\vartheta) = V_-(\vartheta)$.

An example for the decomposition of ξ_- into E- and ambiguous modes is shown in the lower panel of Fig. 1. For large values of ϑ , ξ_-^E differs only little from ξ_- , but their difference increases for smaller ϑ . In particular, ξ_-^E has two roots in the interval $\vartheta \in [\vartheta_{\min}, \vartheta_{\max}]$.

We point out that pure-mode correlation functions equivalent to the foregoing ones were already defined in SEK. However, their expressions in terms of ξ_{\pm} in SEK were considerably

more complicated than the present ones, and therefore, they have not been applied to any data, as far as we know. Our choice of the orthonormality relation, which differs from the one in SEK, allowed us to obtain far more explicit expressions for the pure-mode shear correlation functions, and they are easily applicable to a set of measured ξ_{\pm} , as we show in Sect. 4.

3.3. Comparison with ‘old’ pure-mode shear correlation functions

3.3.1. General considerations

Previously, the CNPT correlation functions that were defined by Crittenden et al. (2002) and Schneider et al. (2002) also yield a mode separation; they are given in terms of the E- and B-mode convergence power spectra $P_{E,B}(\ell)$ through

$$\begin{aligned}\xi_{E,B+}^{\text{CNPT}}(\vartheta) &= \int_0^\infty \frac{d\ell}{2\pi} P_{E,B}(\ell) J_0(\ell\vartheta), \\ \xi_{E,B-}^{\text{CNPT}}(\vartheta) &= \int_0^\infty \frac{d\ell}{2\pi} P_{E,B}(\ell) J_4(\ell\vartheta).\end{aligned}\quad (55)$$

These functions can be expressed solely in terms of the shear correlation functions,

$$\begin{aligned}\xi_{E+}^{\text{CNPT}}(\vartheta) &= \frac{1}{2} \left[\xi_+(\vartheta) + \xi_-(\vartheta) + \int_\vartheta^\infty \frac{d\theta}{\theta} \xi_-(\theta) \left(4 - \frac{12\vartheta^2}{\theta^2} \right) \right], \\ \xi_{E-}^{\text{CNPT}}(\vartheta) &= \frac{1}{2} \left[\xi_+(\vartheta) + \xi_-(\vartheta) + \int_0^\vartheta \frac{d\theta}{\theta^2} \xi_+(\theta) \left(4 - \frac{12\vartheta^2}{\theta^2} \right) \right], \\ \xi_{B+}^{\text{CNPT}}(\vartheta) &= \frac{1}{2} \left[\xi_+(\vartheta) - \xi_-(\vartheta) - \int_\vartheta^\infty \frac{d\theta}{\theta} \xi_-(\theta) \left(4 - \frac{12\vartheta^2}{\theta^2} \right) \right], \\ \xi_{B-}^{\text{CNPT}}(\vartheta) &= \frac{1}{2} \left[\xi_+(\vartheta) - \xi_-(\vartheta) + \int_0^\vartheta \frac{d\theta}{\theta^2} \xi_+(\theta) \left(4 - \frac{12\vartheta^2}{\theta^2} \right) \right].\end{aligned}\quad (56)$$

These can now be compared to the pure-mode correlation functions on a finite interval. We see that the functional form differs in two respects. First, the integrals over the correlation functions ξ_{\pm} only extend over the finite interval for $\xi_{\pm}^{E,B}$, whereas they extend to either 0 or ∞ for $\xi_{E,B\pm}^{\text{CNPT}}$. Second, in the $\xi_{\pm}^{E,B}$ a term is subtracted which corresponds to the ambiguous modes.

Another way to see the difference between the CNPT and the pure-mode correlation functions is by noting that

$$\xi_+(\vartheta) = \xi_{E+}^{\text{CNPT}}(\vartheta) + \xi_{B+}^{\text{CNPT}}(\vartheta); \quad \xi_-(\vartheta) = \xi_{E-}^{\text{CNPT}}(\vartheta) - \xi_{B-}^{\text{CNPT}}(\vartheta), \quad (57)$$

whereas the decomposition into the pure-mode correlation functions is given by Eq. (22).

The $\xi_{E,B\pm}^{\text{CNPT}}$ are unobservable, as they require a measurement of ξ_{\pm} either down to zero separation or up to infinite separation; neither of this is possible. Note that the $\xi_{E,B\pm}^{\text{CNPT}}$ do not account for ambiguous modes, since for an infinite field, there are no ambiguous modes: a constant shear on an infinite field would violate the assumption of statistical isotropy of the random field (whereas on a collection of finite fields, the constant shear can have random magnitude and orientations for each field), and a linear shear field on an infinite field in addition would diverge (see the discussion in Appendix A). The ambiguous mode ξ_+^{amb} is due to the lack of information on ξ_{\pm} for scales $\vartheta > \vartheta_{\text{max}}$, whereas the ξ_-^{amb} is rooted in the missing information from scales $\vartheta < \vartheta_{\text{min}}$.

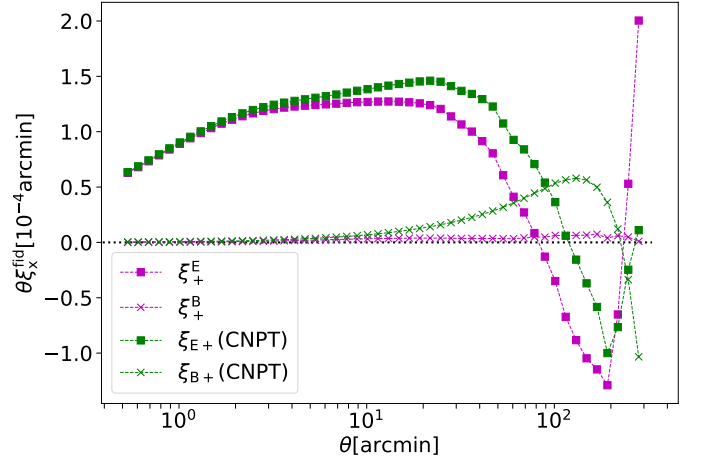


Fig. 2. Measured E-/B-mode correlation functions from SLICS simulations. Both E-modes (squares) and B-modes (crosses) are averaged over 10 shape noise-free lines-of-sight. The pure-mode correlation functions (magenta) are insensitive to information outside of the defined angular separation range, $[0.5', 300']$. The CNPT correlation functions (green) include ambiguous modes and information from outside of the measured range.

We can check that the pure-mode shear correlation functions tend towards the CNPT correlation functions in the limit $\vartheta_{\text{min}} \rightarrow 0$ or $\vartheta_{\text{max}} \rightarrow \infty$. Consider first the ‘+’ modes, and let $\vartheta_{\text{max}} \rightarrow \infty$, which implies also $\bar{\vartheta} \rightarrow \infty$ and $B \rightarrow 1$ such that $(1 - B) = \vartheta_{\text{min}}/\bar{\vartheta}$. In this limit, the function $H_+(\vartheta, \theta)$ tends to a constant, and $S_+(\vartheta) \rightarrow 0$. Furthermore, $H_-(\vartheta, \theta) \rightarrow 0$, due to the factors $(1 - B)^2$ in Eq. (46); correspondingly, $S_-(\vartheta) \rightarrow 0$. Thus, in this limit, the expressions (41) and (42) for $\xi_{\pm}^{E/B}(\vartheta)$ converge to the corresponding ones in Eq. (56). For the ‘-’ modes, we consider $\vartheta_{\text{min}} \rightarrow 0$, implying $B \rightarrow 1$. That means that $K_{\pm}(\vartheta, \theta) \rightarrow 0$, and thus $V_{\pm}(\vartheta) \rightarrow 0$. Hence we see that the expressions (53) and (54) for $\xi_{\pm}^{E/B}(\vartheta)$ converge to the corresponding ones in Eq. (56).

3.3.2. Comparison using SLICS

Asgari et al. (2019) modelled multiple data systematics that may exist in cosmic shear data. They applied these systematics to mock data from SLICS N-body simulations (see their section 6 for details). Ten lines of sight were chosen and the measurements were applied to shape noise-free mock data. Aside from the SEK COSEBIs they measured $\xi_{E/B+}^{\text{CNPT}}$ from these simulations. Here we compare the pure mode correlation functions with their measurements.

Figure 2 compares the measured signal for both the pure-mode and the CNPT correlation functions. The results are shown for the mean of ten lines-of-sight. Here the mock data is free of systematic effects. The measurements are made for 50 logarithmic bins in θ . As can be seen, these two sets of correlation functions match at small separations, while they differ on larger scales; this is because ambiguous modes are not removed from $\xi_{E/B+}^{\text{CNPT}}$. In addition, a theoretical prediction for ξ_- is used beyond $\theta = 300'$, to calculate the integrals in Eq. (56). In particular, we can see that the pure mode ξ_+^B closely recovers the zero B-mode prediction, in contrast to ξ_{B+}^{CNPT} .

We choose the point-spread function leakage, as modelled in Asgari et al. (2019, section 5.1.1), as a test case. This systematics introduces both, artificial E- and B-modes. Figure 3 illustrates the E/B-mode measurements in the left and right panels,

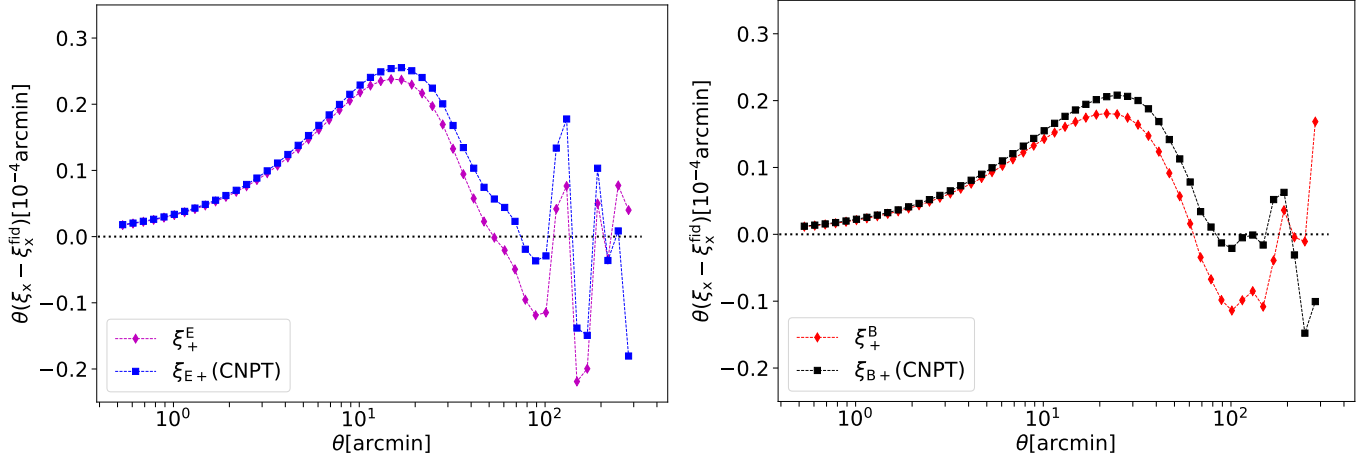


Fig. 3. Comparison between the CNPT and pure-mode correlation functions on systematic induced mock data, averaged over 10 shape noise free lines of sight. The point-spread function (PSF) leakage as modelled by Asgari et al. (2019) is used here. The fiducial no-systematic signal is subtracted from the systematic-induced ones. All measurements are done for 50 logarithmic bins between 0.5 and 300 arcminutes.

respectively. In all cases the impact of the systematic is isolated via subtracting the fiducial no-systematic signal shown in Fig. 2. Again the old and new measurements match at small θ , while they differ at larger scales. The infinite upper bounds in Eq. (56) are more problematic here, since we do not have a theoretical prediction for this systematic effect. Using the pure-mode correlation functions allows us to isolate the scales where systematic effects create B-modes without the need for extrapolating the measurements.

3.4. Consistency checks

Having obtained explicit expressions for the pure-mode shear correlation functions, we shall now apply two checks on their consistency. First, we will show explicitly that they are insensitive to ambiguous modes. Second, we will show that for a pure E-mode shear field, the B-mode correlation functions vanish identically.

3.4.1. Insensitivity of $\xi_{\pm}^{E,B}$ to ambiguous modes

As we mentioned before, some shear modes are neither E- nor B-modes, and they should not affect the $\xi_{\pm}^{E,B}$ functions. For example, a constant shear field, with $\gamma(\theta) = \gamma_0$ leads to a pair of correlation functions $\xi_+(\vartheta) = |\gamma_0|^2$, $\xi_-(\vartheta) = 0$. In this particular case, we find from Eqs. (41, 42) that

$$\xi_+^E(\vartheta) = \xi_+^B(\vartheta) = \frac{1}{2} [\xi_+(\vartheta) - S_+(\vartheta)] , \quad (58)$$

with all other terms vanishing. However, since

$$\int_{\vartheta_{\min}}^{\vartheta_{\max}} \frac{d\vartheta}{\vartheta^2} H_+(\vartheta, \theta) = 1 , \quad (59)$$

$S_+(\vartheta) = |\gamma_0|^2 = \xi_+(\vartheta)$, and $\xi_+^E(\vartheta) = 0 = \xi_+^B(\vartheta)$ in this case. Hence, this ambiguous mode is filtered out. More generally, if we consider a linear shear field, for which $\xi_+(\vartheta) = a + b(\vartheta/\bar{\vartheta})^2$ and $\xi_-(\vartheta) = 0$, then again Eq. (58) holds, and since

$$\int_{\vartheta_{\min}}^{\vartheta_{\max}} \frac{d\vartheta}{\vartheta^2} \left[a + b \left(\frac{\vartheta}{\bar{\vartheta}} \right)^2 \right] H_+(\vartheta, \theta) = a + b \left(\frac{\vartheta}{\bar{\vartheta}} \right)^2 , \quad (60)$$

we again obtain $S_+(\vartheta) = \xi_+(\vartheta)$ and thus $\xi_+^E(\vartheta) = 0 = \xi_+^B(\vartheta)$.

3.4.2. $\xi_{\pm}^B \equiv 0$ for pure E-mode shear

As an important consistency check of the foregoing discussion, we now want to show that the B-mode correlation functions ξ_{\pm}^B identically vanish if the shear field does not contain any B-modes. In this case, the two correlation functions ξ_{\pm} are related through

$$\begin{aligned} \xi_+(\vartheta) &= \xi_-(\vartheta) + \int_{\vartheta}^{\infty} \frac{d\varphi}{\varphi} \xi_-(\varphi) \left(4 - \frac{12\vartheta^2}{\varphi^2} \right) , \\ \xi_-(\vartheta) &= \xi_+(\vartheta) + \int_0^{\vartheta} \frac{d\varphi}{\vartheta^2} \xi_+(\varphi) \left(4 - \frac{12\varphi^2}{\vartheta^2} \right) . \end{aligned} \quad (61)$$

Hence, in the absence of B-modes, Eq. (42) reduces to

$$2\xi_+^B(\vartheta) = \int_{\vartheta_{\min}}^{\infty} \frac{d\vartheta}{\vartheta} \xi_-(\vartheta) \left(4 - \frac{12\vartheta^2}{\vartheta^2} \right) - S_+(\vartheta) + S_-(\vartheta) . \quad (62)$$

In order to show that this vanishes, we first consider the term S_+ and rewrite it with the help of Eq. (61),

$$\begin{aligned} S_+(\vartheta) &= \int_{\vartheta_{\min}}^{\vartheta_{\max}} \frac{d\vartheta}{\vartheta^2} \xi_+(\vartheta) H_+(\vartheta, \theta) \\ &= \int_{\vartheta_{\min}}^{\vartheta_{\max}} \frac{d\vartheta}{\vartheta^2} H_+(\vartheta, \theta) \left[\xi_-(\vartheta) + \int_{\vartheta}^{\vartheta_{\max}} \frac{d\varphi}{\varphi} \xi_-(\varphi) \left(4 - \frac{12\vartheta^2}{\varphi^2} \right) \right. \\ &\quad \left. + \int_{\vartheta_{\max}}^{\infty} \frac{d\varphi}{\varphi} \xi_-(\varphi) \left(4 - \frac{12\vartheta^2}{\varphi^2} \right) \right] \\ &= \int_{\vartheta_{\min}}^{\vartheta_{\max}} \frac{d\vartheta}{\vartheta^2} H_+(\vartheta, \theta) \xi_-(\vartheta) \\ &\quad + \int_{\vartheta_{\min}}^{\vartheta_{\max}} \frac{d\varphi}{\varphi} \xi_-(\varphi) \int_{\vartheta_{\min}}^{\varphi} \frac{d\vartheta}{\vartheta^2} H_+(\vartheta, \theta) \left(4 - \frac{12\vartheta^2}{\varphi^2} \right) \\ &\quad + \int_{\vartheta_{\min}}^{\vartheta_{\max}} \frac{d\vartheta}{\vartheta^2} H_+(\vartheta, \theta) \int_{\vartheta_{\max}}^{\infty} \frac{d\varphi}{\varphi} \xi_-(\varphi) \left(4 - \frac{12\vartheta^2}{\varphi^2} \right) , \end{aligned} \quad (63)$$

where the function $H_+(\vartheta, \theta)$ is given by Eq. (45), and in the second step we have changed the order of integration, subject to the constraint $\vartheta_{\min} \leq \vartheta \leq \varphi \leq \vartheta_{\max}$. Thus, we have rewritten S_+ solely in terms of ξ_- , as are the other terms in Eq. (62). One finds that

$$\int_{\vartheta_{\min}}^{\vartheta_{\max}} \frac{d\vartheta}{\vartheta^2} H_+(\vartheta, \theta) \left(4 - \frac{12\vartheta^2}{\varphi^2} \right) = 4 - \frac{12\vartheta^2}{\varphi^2} , \quad (64)$$

which shows that the final term in Eq. (63) cancels the first term on the r.h.s. of Eq. (62). Hence, ξ_+^B does not have any contributions of ξ_- from outside the considered interval. The remaining terms are

$$2\xi_+^B(\vartheta) = \int_{\vartheta_{\min}}^{\vartheta_{\max}} \frac{d\theta}{\theta} \xi_-(\theta) \left[\left(\frac{\theta}{\vartheta} \right)^2 H_+(\vartheta, \theta) + \int_{\vartheta_{\min}}^{\theta} \frac{d\varphi}{\vartheta^2} \varphi H_+(\vartheta, \varphi) \left(4 - \frac{12\varphi^2}{\theta^2} \right) - H_-(\vartheta, \theta) \right], \quad (65)$$

where the function $H_-(\vartheta, \theta)$ is given by Eq. (46). Carrying out the φ -integral, one can show that the bracket in Eq. (65) vanishes identically, and thus $\xi_+^B(\vartheta) \equiv 0$ in the absence of B-modes.

Similarly, we find from Eqs. (54) and (61) in the case of vanishing B-modes:

$$2\xi_-^B(\vartheta) = \int_{\vartheta_{\min}}^{\vartheta_{\max}} \frac{d\theta}{\vartheta^2} \xi_+(\theta) [K_-(\vartheta, \theta) - K_+(\vartheta, \theta)] - \int_0^{\vartheta_{\min}} \frac{d\theta}{\vartheta^2} \xi_+(\theta) \left(4 - \frac{12\theta^2}{\vartheta^2} \right) + \int_{\vartheta_{\min}}^{\vartheta_{\max}} \frac{d\theta}{\vartheta^2} K_-(\vartheta, \theta) \int_0^{\theta} \frac{d\varphi}{\theta^2} \varphi \xi_+(\varphi) \left(4 - \frac{12\varphi^2}{\theta^2} \right). \quad (66)$$

The last integral is then split up into one from 0 to ϑ_{\min} , and one from ϑ_{\min} to θ . For the former one, we note the result that

$$\int_{\vartheta_{\min}}^{\vartheta_{\max}} \frac{d\theta}{\theta} K_-(\vartheta, \theta) \left(4 - \frac{12\varphi^2}{\theta^2} \right) = \frac{\vartheta^2}{\vartheta^2} \left(4 - \frac{12\varphi^2}{\vartheta^2} \right), \quad (67)$$

so that the corresponding θ -integral just cancels the second term in Eq. (66). Hence, $\xi_-^B(\vartheta)$ contains no contribution from scales outside the angular interval considered. For the θ -integration of the second φ -integral, we change the order of integration, subject to $\vartheta_{\min} \leq \varphi \leq \theta \leq \vartheta_{\max}$, to get

$$2\xi_-^B(\vartheta) = \int_{\vartheta_{\min}}^{\vartheta_{\max}} \frac{d\theta}{\vartheta^2} \xi_+(\theta) \left[K_-(\vartheta, \theta) - K_+(\vartheta, \theta) + \int_{\theta}^{\vartheta_{\max}} \frac{d\varphi}{\varphi} K_-(\vartheta, \varphi) \left(4 - \frac{12\theta^2}{\varphi^2} \right) \right] \quad (68)$$

One can show that the term in the bracket is identically zero, which shows that $\xi_-^B(\vartheta) \equiv 0$ for the case that the shear field has no B-mode contribution.

3.5. Relation to the power spectrum

We now consider the relation between the shear power spectra and the pure-mode shear correlation functions. The $\xi_{\pm}(\vartheta)$ are related to the E- and B-mode power spectra $P_E(\ell)$ and $P_B(\ell)$ by

$$\begin{aligned} \xi_+(\vartheta) &= \int_0^{\infty} \frac{d\ell}{2\pi} J_0(\ell\vartheta) [P_E(\ell) + P_B(\ell)]; \\ \xi_-(\vartheta) &= \int_0^{\infty} \frac{d\ell}{2\pi} J_4(\ell\vartheta) [P_E(\ell) - P_B(\ell)]. \end{aligned} \quad (69)$$

The expressions (41, 42, 53, 54) show that $\xi_{\pm}^{E/B}(\vartheta)$ are linear in the ξ_{\pm} , and hence can be expressed in the form

$$\begin{aligned} \xi_{\pm}^E(\vartheta) &= \int_0^{\infty} \frac{d\ell}{2\pi} \ell [W_{\pm E}^E(\ell, \vartheta) P_E(\ell) + W_{\pm B}^E(\ell, \vartheta) P_B(\ell)]; \\ \xi_{\pm}^B(\vartheta) &= \int_0^{\infty} \frac{d\ell}{2\pi} \ell [W_{\pm E}^B(\ell, \vartheta) P_E(\ell) + W_{\pm B}^B(\ell, \vartheta) P_B(\ell)]. \end{aligned} \quad (70)$$

We start with ξ_{\pm}^E , for which the coefficients read

$$\begin{aligned} W_{+E}^E(\ell, \vartheta) &= \frac{1}{2} \left[J_0(\ell\vartheta) + J_4(\ell\vartheta) + \int_{\vartheta}^{\vartheta_{\max}} \frac{d\theta}{\theta} J_4(\ell\theta) \left(4 - \frac{12\theta^2}{\vartheta^2} \right) - \int_{\vartheta_{\min}}^{\vartheta_{\max}} \frac{d\theta}{\vartheta^2} J_0(\ell\theta) H_+(\vartheta, \theta) - \int_{\vartheta_{\min}}^{\vartheta_{\max}} \frac{d\theta}{\theta} J_4(\ell\theta) H_-(\vartheta, \theta) \right]; \\ W_{+B}^E(\ell, \vartheta) &= \frac{1}{2} \left[J_0(\ell\vartheta) - J_4(\ell\vartheta) - \int_{\vartheta}^{\vartheta_{\max}} \frac{d\theta}{\theta} J_4(\ell\theta) \left(4 - \frac{12\theta^2}{\vartheta^2} \right) - \int_{\vartheta_{\min}}^{\vartheta_{\max}} \frac{d\theta}{\vartheta^2} J_0(\ell\theta) H_+(\vartheta, \theta) + \int_{\vartheta_{\min}}^{\vartheta_{\max}} \frac{d\theta}{\theta} J_4(\ell\theta) H_-(\vartheta, \theta) \right]. \end{aligned}$$

We expect that the latter coefficient vanishes, since the pure E-mode correlation function should not depend on the B-mode power spectrum. Indeed, it can be shown that $W_{+B}^E(\ell, \vartheta) \equiv 0$. By adding the previous two equations, we can simplify the expression for $W_{+E}^E(\ell, \vartheta)$ to

$$\begin{aligned} W_{+E}^E(\ell, \vartheta) &= J_0(\ell\vartheta) - \int_{\vartheta_{\min}}^{\vartheta_{\max}} \frac{d\theta}{\vartheta^2} J_0(\ell\theta) H_+(\vartheta, \theta) \\ &= J_0(\ell\vartheta) - \frac{(1+B)}{4B^2\ell\vartheta} \left[3 \left(\frac{\vartheta}{\vartheta} \right)^2 - (3-2B+3B^2) \right] J_1(\ell\vartheta_{\max}) \\ &\quad - \frac{(1-B)}{4B^2\ell\vartheta} \left[3 \left(\frac{\vartheta}{\vartheta} \right)^2 - (3+2B+3B^2) \right] J_1(\ell\vartheta_{\min}) \\ &\quad + \frac{3}{4B^3(\ell\vartheta)^2} \left[\left(\frac{\vartheta}{\vartheta} \right)^2 - (1+B^2) \right] \\ &\quad \times \left[(1+B)^2 J_2(\ell\vartheta_{\max}) - (1-B)^2 J_2(\ell\vartheta_{\min}) \right]. \end{aligned} \quad (71)$$

We first note that the function W_{+E}^E does not only depend on the product $\ell\vartheta$, as was the case for the corresponding filter for ξ_+ . Since the pure-mode correlation functions depend on the angular interval $\vartheta_{\min} \leq \vartheta \leq \vartheta_{\max}$, the filter W_{+E}^E has an explicit dependence on the interval boundaries, expressed through B , ϑ and the arguments of the Bessel functions. The additional terms in W_{+E}^E filter out the ambiguous modes. In fact, since for small ℓ , $W_{+E}^E(\ell, \vartheta) \propto \ell^4$, low- ℓ modes in the power spectrum are strongly suppressed.

The foregoing fact is an important observation. The filter relating ξ_+ to the power spectra is $J_0(\ell\vartheta)$, which tends to unity as $\ell \rightarrow 0$. Hence, ξ_+ is very sensitive to small- ℓ power, i.e., to large-scale modes. The fact that the filter W_{+E}^E has a leading ℓ^4 dependence shows that the sensitivity of ξ_+ to large-scale modes is due solely to the ambiguous modes in ξ_+ .

Turning to ξ_{\pm}^B , it is straightforward to see that $W_{+E}^B(\ell, \vartheta) = W_{+B}^E(\ell, \vartheta) = 0$ and $W_{+B}^B(\ell, \vartheta) = W_{+E}^E(\ell, \vartheta)$. Thus, the pure B-mode correlation function is independent of the E-mode power spectrum, and the relation between ξ_{\pm}^B and P_B is the same as between ξ_{\pm}^E and P_E .

The filter functions for ξ_{\pm}^E are

$$\begin{aligned} W_{-E/B}^E(\ell, \vartheta) &= \frac{1}{2} \left[J_0(\ell\vartheta) \pm J_4(\ell\vartheta) + \int_{\vartheta_{\min}}^{\vartheta} \frac{d\theta}{\vartheta^2} J_0(\ell\theta) \left(4 - \frac{12\theta^2}{\vartheta^2} \right) - \int_{\vartheta_{\min}}^{\vartheta_{\max}} \frac{d\theta}{\vartheta^2} J_0(\ell\theta) K_+(\vartheta, \theta) \mp \int_{\vartheta_{\min}}^{\vartheta_{\max}} \frac{d\theta}{\vartheta^2} J_4(\ell\theta) K_-(\vartheta, \theta) \right], \end{aligned}$$

where the upper (lower) signs apply for W_{-E}^E (W_{-B}^E). We find that $W_{-B}^E(\ell, \vartheta) \equiv 0$, as expected, i.e., the B-mode power does not

contribute to the pure E-mode correlation function ξ_{-}^E . Taking the sum of the two filter functions, we find that

$$\begin{aligned} W_{-E}^E(\ell, \vartheta) &= J_0(\ell\vartheta) + \int_{\vartheta_{\min}}^{\vartheta} \frac{d\theta}{\vartheta^2} J_0(\ell\theta) \left(4 - \frac{12\theta^2}{\vartheta^2}\right) \\ &\quad - \int_{\vartheta_{\min}}^{\vartheta_{\max}} \frac{d\theta}{\vartheta^2} J_0(\ell\theta) K_+(\vartheta, \theta) \\ &= J_4(\ell\vartheta) + \frac{(1-B^2)}{4B^2\ell\vartheta} \left[a_{-1}^{\min} J_1(\ell\vartheta_{\min}) + a_{-1}^{\max} J_1(\ell\vartheta_{\max}) \right] \\ &\quad + \frac{3(1-B^2)^2}{4B^3(\ell\vartheta)^2} \left[a_{-2}^{\min} J_2(\ell\vartheta_{\min}) + a_{-2}^{\max} J_2(\ell\vartheta_{\max}) \right] \end{aligned} \quad (72)$$

where the coefficients are

$$\begin{aligned} a_{-1}^{\min} &= (1+B) \left[3(1-B^2)^2 \left(\frac{\vartheta}{\vartheta}\right)^{-4} - (3-2B+3B^2) \left(\frac{\vartheta}{\vartheta}\right)^{-2} \right]; \\ a_{-1}^{\max} &= (1-B) \left[3(1-B^2)^2 \left(\frac{\vartheta}{\vartheta}\right)^{-4} - (3+2B+3B^2) \left(\frac{\vartheta}{\vartheta}\right)^{-2} \right]; \\ a_{-2}^{\min} &= (1+B)^2(1-4B+B^2) \left(\frac{\vartheta}{\vartheta}\right)^{-4} - (1-B^2) \left(\frac{\vartheta}{\vartheta}\right)^{-2}; \\ a_{-2}^{\max} &= (1+B^2) \left(\frac{\vartheta}{\vartheta}\right)^{-2} - (1-B)^2(1+4B+B^2) \left(\frac{\vartheta}{\vartheta}\right)^{-4}. \end{aligned} \quad (73)$$

Finally, we find $W_{-E}^B(\ell, \vartheta) \equiv 0$, again as expected since the correlation function $\xi_{-}^B(\vartheta)$ should not depend on the E-mode power spectrum, and $W_{-B}^B(\ell, \vartheta) = W_{-E}^E(\ell, \vartheta)$. Thus, of the eight filter functions $W_{\pm E/B}^{E/B}$, four are identically zero, and the remaining four are pairwise identical, so that only the two given in Eqs. (71) and (72) need to be evaluated.

We note that as $\vartheta_{\min} \rightarrow 0$, $\vartheta_{\max} \rightarrow \infty$, $W_{+E}^E(\ell, \vartheta) \rightarrow J_0(\ell\vartheta)$ and $W_{-E}^E(\ell, \vartheta) \rightarrow J_4(\ell\vartheta)$, due to the behavior of the Bessel functions for small and large arguments. Hence, in this case the relation between the pure-mode shear correlation functions and the power spectra reduces to that of the CNPT correlation functions.

Finally, from the decomposition (22) of the correlation functions and the results of this subsection, we find the relation between the ambiguous modes and the power spectra,

$$\begin{aligned} \xi_{+}^{\text{amb}}(\vartheta) &= \int \frac{d\ell}{2\pi} \left[J_0(\ell\vartheta) - W_{+E}^E(\ell, \vartheta) \right] [P_E(\ell) + P_B(\ell)], \\ \xi_{-}^{\text{amb}}(\vartheta) &= \int \frac{d\ell}{2\pi} \left[J_4(\ell\vartheta) - W_{-E}^E(\ell, \vartheta) \right] [P_E(\ell) - P_B(\ell)]. \end{aligned} \quad (74)$$

Given that both of the $\xi_{\pm}^{\text{amb}}(\vartheta)$ are characterized by only two coefficients, it is obvious that one can find many combinations of E-/B-mode power spectra for which these coefficients are the same. Therefore, these ambiguous mode correlation functions can result from different combinations of E- and B-modes. We give some specific examples for this in Appendix A.3.

4. KiDS-1000 measurements

4.1. Data description

The Kilo Degree Survey is designed with weak gravitational lensing applications in mind. Its data, therefore, benefits from high-quality images in the *r*-band (mean seeing of 0.7 arcseconds), which is used for the shape measurements (Giblin et al. 2021). In addition, all galaxies have matched depth images in optical, *ugri*, and near-infrared photometric bands, *ZYJHK_s*.

The five near-infrared bands are observed by VIKING (the VISTA Kilo-degree INfrared Galaxy survey; Edge et al. 2013). These nine bands are used to estimate photometric redshifts for all galaxies that contribute to the cosmic shear signal. The fourth KiDS data release includes 1006 square degrees of images (Kuijken et al. 2019). The data is divided into five tomographic bins before two-point correlation functions are measured for the 15 distinct combinations of redshift bins¹. The redshift distribution for each tomographic bin is calibrated using KiDS+VIKING-like observations of fields containing spectroscopic samples (Hildebrandt et al. 2021).

The theoretical predictions are calculated with the KiDS Cosmology Analysis Pipeline² (KCAP) which is built from the modular cosmology pipeline, CosmoSIS³ (Zuntz et al. 2015). The primordial power spectrum is estimated using the CAMB Boltzmann code (Lewis et al. 2000). Its non-linear evolution is calculated via the augmented halo model approach of Mead et al. (2015), which also accounts for the impact of baryon feedback from active galactic nuclei. We model the intrinsic alignments of galaxies with the non-linear linear alignment model of Bridle & King (2007, NLA; see also Hirata & Seljak 2004) and use a modified Limber approximation (LoVerde & Afshordi 2008) to project the three-dimensional power spectra to two dimensions, $P_E(\ell)$. This is then used to make predictions for the pure mode correlation functions and the new dimensionless COSEBIs.

4.2. COSEBIs and pure-mode correlations for KiDS-1000

We measure the new dimensionless logarithmic COSEBIs (see Appendix B) by integrating over the measured ξ_{\pm} .⁴ The pure-mode correlation functions are determined by integrating over the ξ_{\pm} , according to the relations given in Sect. 3.2. As a consistency check, we also calculated $\xi_{\pm}^{E/B}$ using Eqs. (23) and (24), using the first 20 COSEBIs modes. We find that the sums in Eqs. (23) and (24) converge to the previous result after about the first 5 COSEBI modes.

Figures 4, 5 and 6 display the measured dimensionless COSEBIs, ξ_{\pm}^E and ξ_{\pm}^B for the angular separation range of 0.5 to 300 arcminutes. In these figures, the error bars are drawn from the diagonal of their respective covariance matrix. Each panel belongs to a pair of redshift bins. The theoretical curves are calculated using the best-fitting flat Λ CDM cosmology to the KiDS-1000 cosmic shear data (SEK COSEBIs, Asgari et al. 2021) whose parameter values are given in Table 1. Although not listed here we also fix the mean redshift displacement parameters to their best-fitting values as estimated in Asgari et al. (2021). In all cases, the theory values are connected to each other for ease of comparison, although they are all discrete with the exception of the unbinned theory curves (blue) in Fig 5. For COSEBIs this is true by definition, while for $\xi_{\pm}^{E/B}$ the binning of the data requires that the theoretical predictions are also binned (orange dashed curves).

4.3. Covariances and Fisher analysis

We first derive the covariance matrix for the new COSEBIs using the methodology detailed in Joachimi et al. (2021) and Appendix A of Asgari et al. (2020). The corresponding correlation

¹ https://github.com/KiDS-WL/Cat_to_Obs_K1000_P1

² <https://github.com/KiDS-WL/kcap>

³ <https://bitbucket.org/joezuntz/cosmosis/wiki/Home>

⁴ We refer the reader to Asgari et al. (2017) for details on this conversion from ξ_{\pm} to COSEBIs.

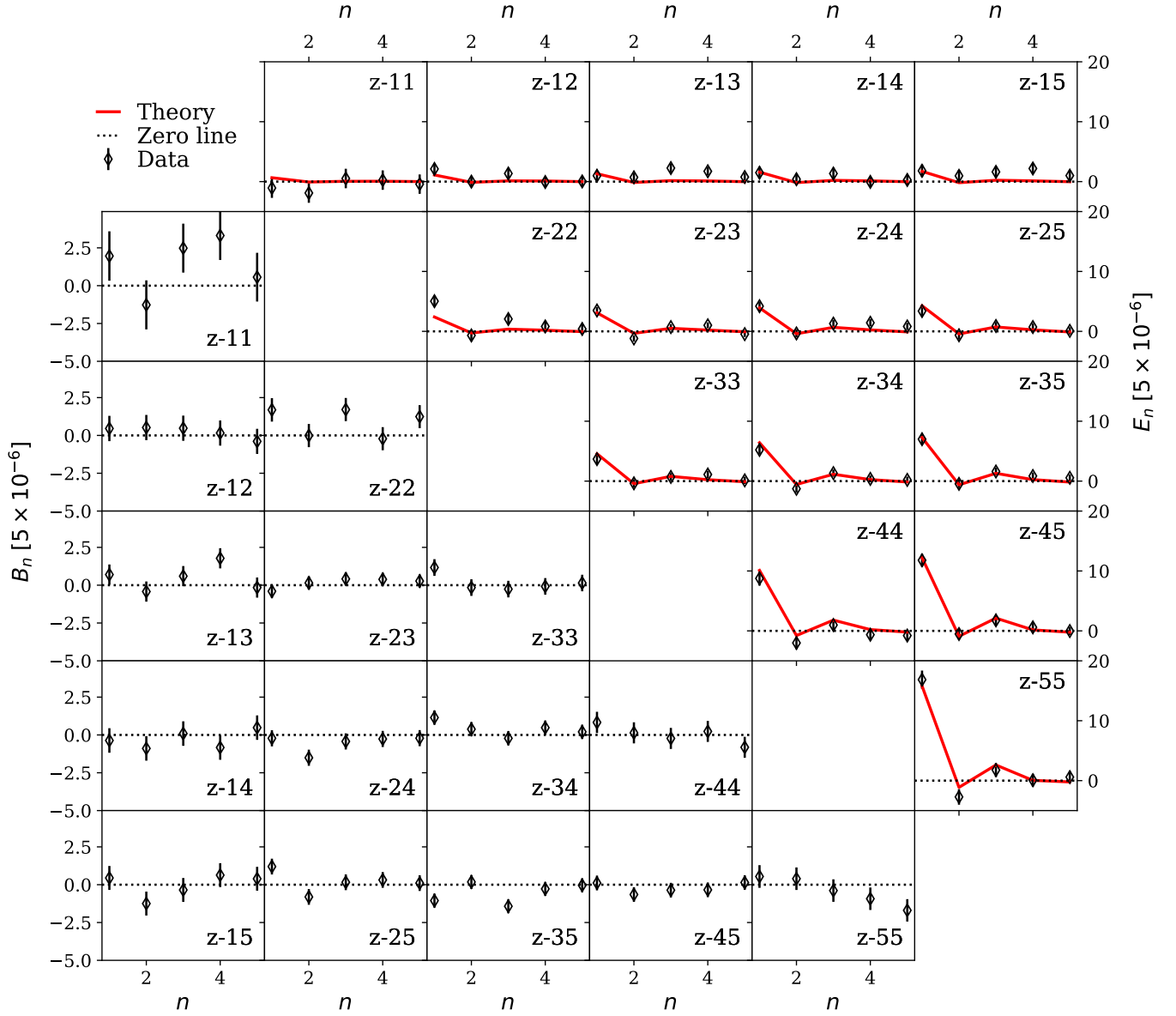


Fig. 4. Dimensionless logarithmic COSEBIs (see Appendix B) measurements from KiDS-1000 data. The E/B-modes are shown in the top/bottom triangles. Each panel depicts results for a pair of redshift bins, $z-ij$. The solid red curves correspond to the best fitting model to the SEK COSEBIs as analysed in Asgari et al. (2021, compare with their figure 3). The B-modes are consistent with zero (p -value = 0.36) and the best-fit model describes the data very well (p -value = 0.2). Note that the COSEBIs modes are discrete and the points are connected to each other for visual aid.

matrix is shown in the left panel of Fig. 7 and compared to the correlation matrix for the SEK COSEBIs shown on the right. As can be seen, the dimensionless COSEBIs are considerably less correlated, making them more mutually independent.

We then estimate the covariance matrices for the pure-mode correlation functions, making use of the linear relation between them and the COSEBIs given by Eqs. (23) and (24). The correlation coefficients are shown in Fig. 8 for $\xi_{\pm}^{E/B}$.

Although the theoretical curves are not fitted to the data in Figs. 4 and 5 we see that they describe the data very well.⁵ We

estimate the goodness-of-fit using the probability to exceed the measured χ^2 , i.e., the p -value. Following Joachimi et al. (2021) we assume that the effective number of free parameters is 4.5 and set the degrees of freedom to the number of data points, minus 4.5. We then find that all p -values are above 0.09 (p -values for each data vector are reported in the caption of their figure). This is to be expected as the fit is done to the SEK COSEBIs (p -value = 0.16), which separate E/B-modes on the same angular range. Figure 6 and the bottom panels of Fig. 4, depict the B-mode signals. We find that the B-modes are consistent with zero in all cases and all p -values are above 0.1. We also report the p -values for individual pairs of redshift bins in Fig. 6, which can be compared with the results of Giblin et al. (2021) who used SEK COSEBIs to determine the significance of B-modes in KiDS-1000 data. Note that as demonstrated in Asgari et al. (2019) the significance of the B-modes has a non-trivial dependence on the way the data is binned or equivalently the number

⁵ In principle, as mentioned before, the dimensionless COSEBIs and the pure-mode correlation functions should yield exactly the same result as using the SEK COSEBIs, as all these quantities contain the same information. In practice, however, the results will slightly differ, due to the use of a finite number of COSEBI modes and a finite number of θ -bins for the correlation functions.

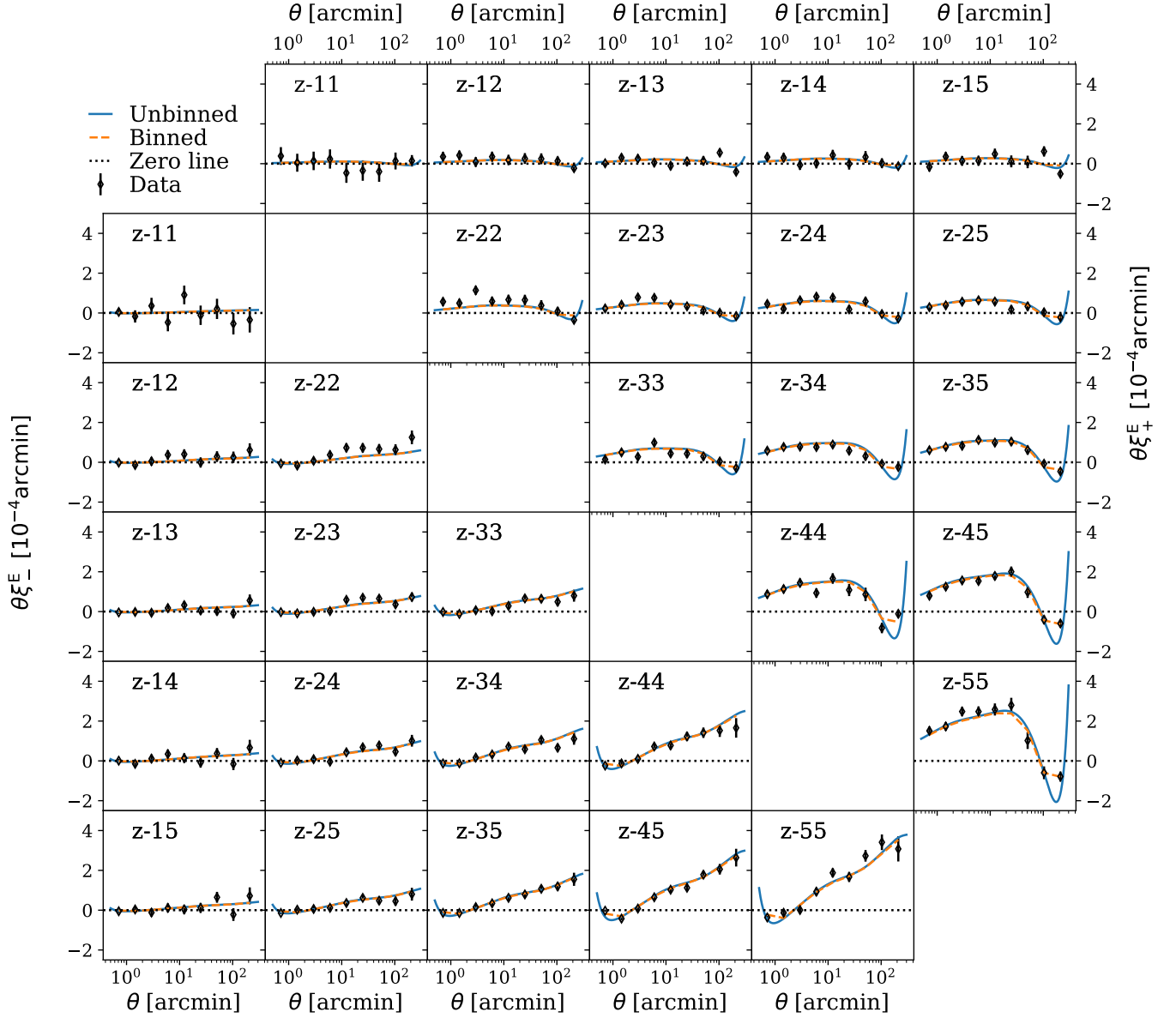


Fig. 5. KiDS-1000 pure E-mode correlation functions. The top and bottom panels show ξ_+^E and ξ_-^E , respectively. The theory curve is shown for both unbinned (blue solid) and binned (orange dashed) cases. The data points should be compared with the binned curve. The model is calculated assuming the best-fitting standard cosmology to SEK COSEBIs (Asgari et al. 2021). Although the model is not fitted to this data vector we find that it agrees with the data very well (p -value = 0.09 for ξ_+^E and 0.28 for ξ_-^E).

of COSEBI modes that are used⁶, as well as the type of systematic effects that exist in the data. While certain systematics produce E- and B-modes on similar angular separations (see for example the impact of PSF-leakage in Fig. 3), others such as a CCD-chip bias that produces a repeating pattern in the images (see for example Asgari et al. 2019, regular pattern Figures 9 and 10), show a different scale dependence for E- and B-modes. Therefore, similar to COSEBIs here we recommend to use multiple binning schemes to test the significance of B-modes. In fact, we find similar trends to Giblin et al. (2021) depending on the number of θ -bins. When we divide the $[0.5', 300']$ range into 20 θ -bins we find that bin 55 has the smallest p -value = 0.04,

whereas dividing the same range into 5 bins results in smaller p -values for redshift bin combinations 22 and 35. Nevertheless, all p -values are above the 0.01 threshold and thus we conclude that the B-modes are insignificant. We also find that by increasing the number of θ bins, the p -values resulting from ξ_+^B and ξ_-^B become very similar, confirming that these two functions contain the same information.

We compare the information content of the pure mode correlation function, ξ_+^E with the SEK COSEBIs, in Fig. 9. We use a Fisher formalism and assume the fiducial values in Table 1 for model parameters. As was shown in Asgari et al. (2021), we expect to have meaningful constraints only for the structure growth parameter S_8 and the amplitude of the intrinsic alignments A_{IA} . Therefore, we fix all other parameters and only show the 1 and 2σ contours for S_8 and A_{IA} . We see that the information content of ξ_+^E and COSEBIs is identical, and conclude that there is no extra cosmological information to be gained from the pure-

⁶ The number of COSEBI modes and theta bins do not have a one-to-one relation. However, the higher COSEBI modes are more sensitive to smaller scale variations across the full range of the correlation functions. These variations are lost when data is binned coarsely.

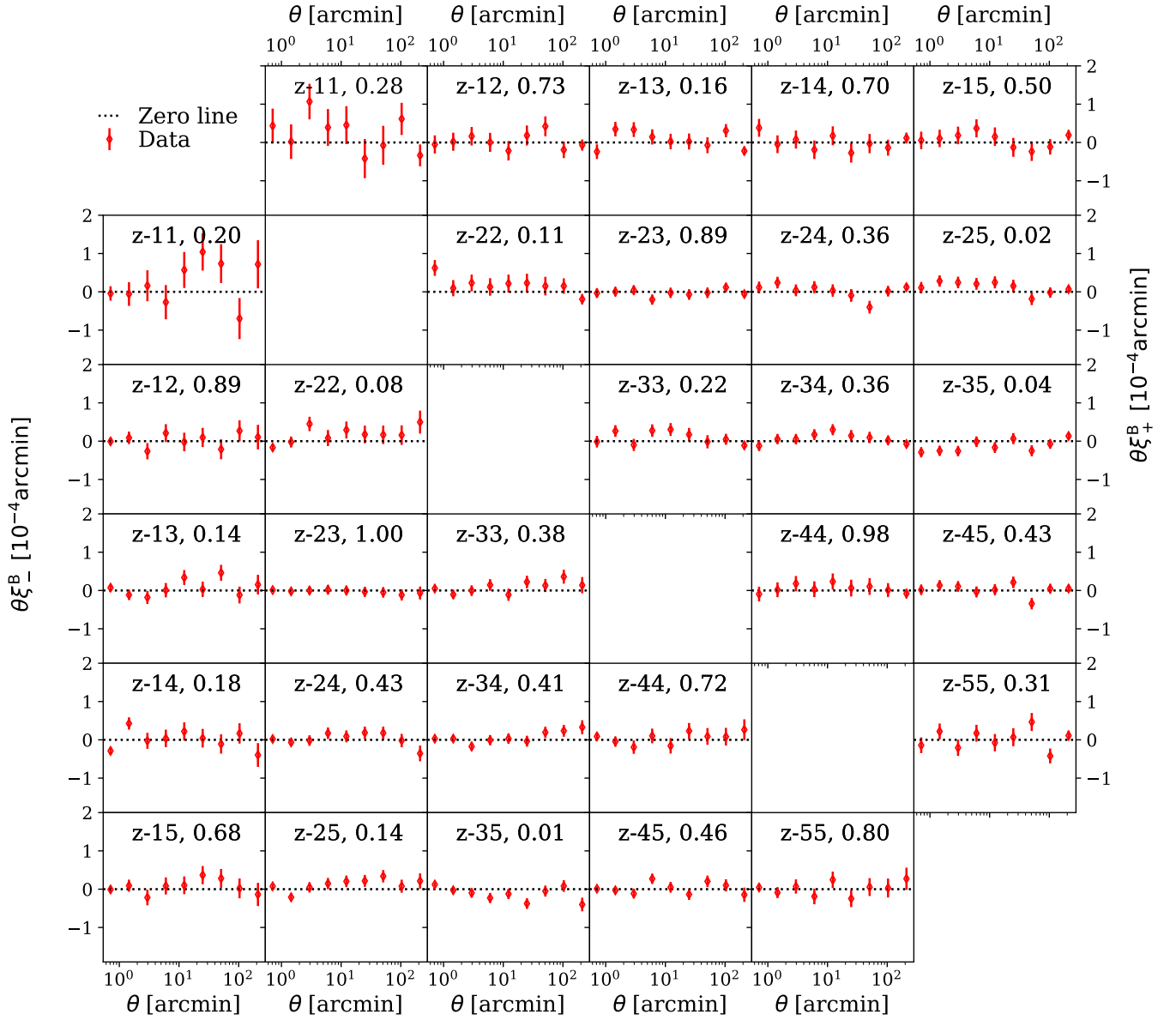


Fig. 6. KiDS-1000 pure B-mode correlation functions. ξ_+^B is displayed in the top panels, while ξ_-^B is shown in the bottom ones. Each panel represents measurements for a pair of redshift bins $z - ij$ and its associated p -value. We find that the B-modes are consistent with zero when we consider the full data vectors (p -value = 0.11 for ξ_+^B and 0.20 for ξ_-^B).

mode correlation functions. This is also true when we compare the dimensionless and SEK COSEBIs Fisher matrices. This is to be expected, as both methods make use of the E-mode information that is available in the given angular interval. With the Fisher analysis we can also estimate the expected errors on the measured parameters. We find that the error on S_8 is 0.014 and on A_{IA} is 0.274, both are slightly smaller than the full likelihood analysis of Asgari et al. (2021), as expected.

5. Summary and discussion

In this paper, we derived pure-mode shear correlation functions which can be obtained from the measured shear correlations $\xi_{\pm}(\vartheta)$ on a finite interval $0 < \vartheta_{\min} \leq \vartheta \leq \vartheta_{\max} < \infty$. This was achieved by redefining the orthonormality relation of COSEBIs, which allowed us the construction of two complete sets of orthonormal weight functions $T_{\pm\mu}(\vartheta)$ on this finite interval; explicit expressions for these new weight functions are given in

Appendix B. Two of these weight functions correspond to ambiguous modes, and with the remaining ones, the E-/B-mode separating COSEBIs were defined. Owing to the completeness of these function sets, we could decompose the shear correlation functions into their E- and B-mode correlations $\xi_{\pm}^{E/B}(\vartheta)$ and their contribution by ambiguous modes (see Eq. 22). These different components can be straightforwardly determined from the $\xi_{\pm}(\vartheta)$ measured on a finite interval, in contrast to the CNPT correlation functions (see Sect. 3.3) which require extrapolation or modelling of ξ_{\pm} for separations smaller or larger than where measurements of ξ_{\pm} are available. Hence, there is no reason anymore to use these CNPT correlation functions. Only in the limit of $\vartheta_{\min} \rightarrow 0$ and $\vartheta_{\max} \rightarrow \infty$ do they agree with mode-separating ones.

These new correlation functions allow the study of E- and B-mode second-order shear as a function of angular scale. Hence, they should serve as a diagnostic for the angular dependence of

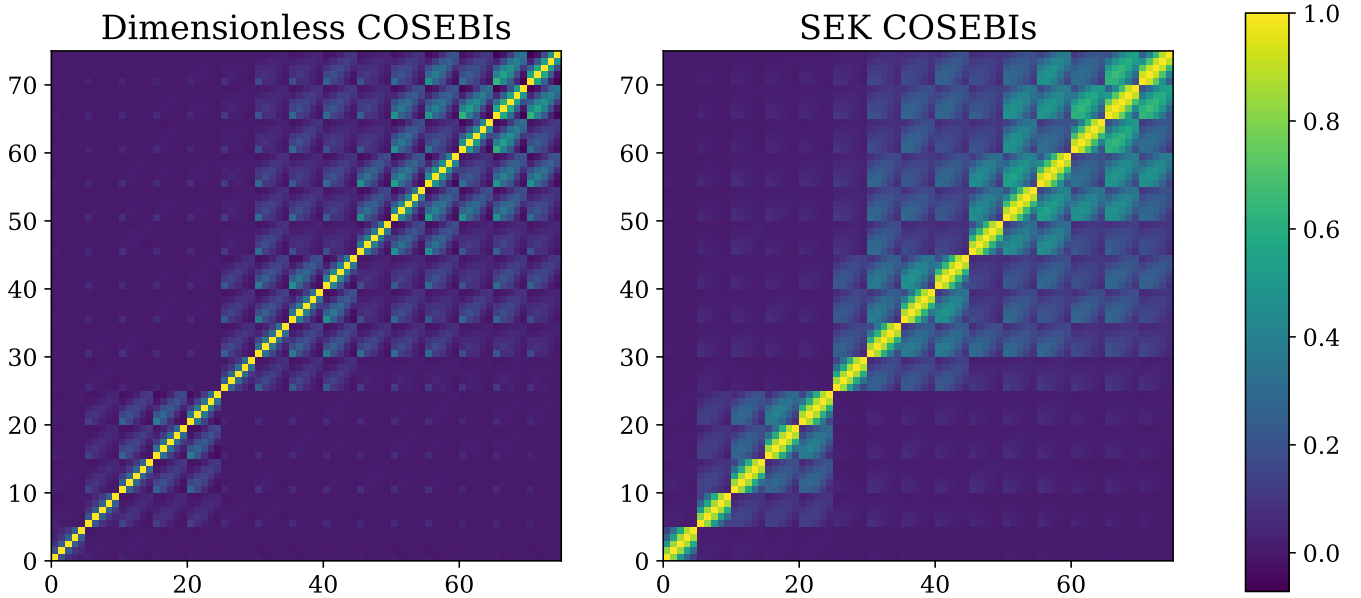


Fig. 7. Correlation matrices for new (left) and old (right) logarithmic COSEBIs. Here we illustrate the correlation matrices for the first 5 COSEBI modes. Each block of 5×5 shows the values for one pair of redshift bins, starting with the lowest bins at the bottom left corner.

potential B-modes in a survey. To illustrate this, we have applied the pure-mode correlation functions to simulation data, without and with systematics added, and compared the results with our earlier analysis (Asgari et al. 2019).

We applied the newly constructed dimensionless COSEBIs to the KiDS-1000 tomographic cosmic shear dataset, for which we also computed the pure-mode shear correlation functions. Calculating the covariance of the COSEBIs and the binned $\xi_{\pm}^{E/B}$, we showed that their measured values are fully consistent with the best-fitting model parameters obtained in Asgari et al. (2021), exhibiting only very small differences in the p -values. Using the Fisher analysis, we also showed that the results on the two parameters best constrained by the cosmic shear data (S_8 and A_{IA}) are indistinguishable between the COSEBIs and the pure-mode correlation functions – as was to be expected. The discrete nature of the COSEBIs make them the more convenient quantities for a cosmological analysis.

In Appendix A, we provided a few illustrative examples of ambiguous modes in the shear correlation function, i.e., modes which can not be uniquely attributed either to E- or B-modes. Incorporation of such modes into a cosmological analysis bears the possibility that they are affected by a contribution coming from B-modes, and hence the analysis may be biased. We therefore caution against the use of ambiguous modes for deriving constraints on model parameters; instead, employing COSEBIs for that purpose avoids this potential trap. We note that the sensitivity of $\xi_{+}(\theta)$ to low- ℓ power, due to the filter $J_0(\ell\theta)$ relating them, is solely due to ambiguous modes; the corresponding filter function for the pure-mode correlation has an ℓ^4 -dependence for $\ell \rightarrow 0$.

As was shown in Asgari et al. (2012), if one assumes that the ambiguous modes are pure E-modes, then they contain additional cosmological information – this corresponds to the case termed ‘full COSEBIs’ in Asgari et al. (2012). The relative amount of information in these ambiguous modes depends on the angular range ϑ_{\min} and ϑ_{\max} , and presumably on the number of cosmological parameters. However, as was made clear above, from the measurement of the correlation functions on this

finite interval, one cannot tell whether these ambiguous modes are pure E-modes, or whether B-modes are mixed in. We therefore strongly advise against the use of ambiguous modes for cosmological parameter inference.

The same statement holds for the correlation functions ξ_{\pm} ; using them for cosmological parameter estimates, one needs to (implicitly) assume that they are pure E-mode functions, which can not be verified from a measurement on a finite angular separation interval. Thus, such estimates may contain an unknown level of systematics due to B-modes which remain undetected by the COSEBIs, but are hidden in the ambiguous modes.

Finally, we showed in Appendix C that the COSEBIs defined on a subinterval of the original one can be obtained as linear combinations of the original COSEBIs. This was to be expected, since these original COSEBIs contain the full E-/B-mode separable information about second-order shear statistics. We thus conclude that it suffices to consider the COSEBIs on the full angular range where the ξ_{\pm} are measured, without the need to consider sub-intervals. The lack of localized information in the individual COSEBIs is remedied by the use of the pure-mode shear correlation functions derived here.

Acknowledgements. This work was supported by the Deutsche Forschungsgemeinschaft with the grant SCHN342-13 and the Heisenberg grant Hi 1495/5-1, the European Research Council under grants number 647112 and 770935, by an STFC Ernest Rutherford Fellowship (project reference ST/S004858/1), by the Max Planck Society and the Alexander von Humboldt Foundation in the framework of the Max Planck-Humboldt Research Award endowed by the Federal Ministry of Education and Research ERC with the Consolidator Grant No. 770935, by the Vici grant 639.043.512, financed by the Netherlands Organisation for Scientific Research (NWO), by the Royal Society and Imperial College, by the CMS-CSST-2021-A01, NSFC of China under grant 11973070, the Shanghai Committee of Science and Technology grant No.19ZR1466600 and Key Research Program of Frontier Sciences, CAS, Grant No. ZDBS-LY-7013, and the Leverhulme Trust. Based on observations made with ESO Telescopes at the La Silla Paranal Observatory under programme IDs 177.A-3016, 177.A-3017, 177.A-3018 and 179.A-2004, and on data products produced by the KiDS consortium. The KiDS production team acknowledges support from: Deutsche Forschungsgemeinschaft, ERC, NOVA and NWO-M grants; Target; the University of Padova, and the University Federico II (Naples).

Author contributions: All authors contributed to the development and writing of this paper. The authorship list is given in two groups: the lead authors (PS,MA,YNJ) followed by an alphabetical group that covers those who have

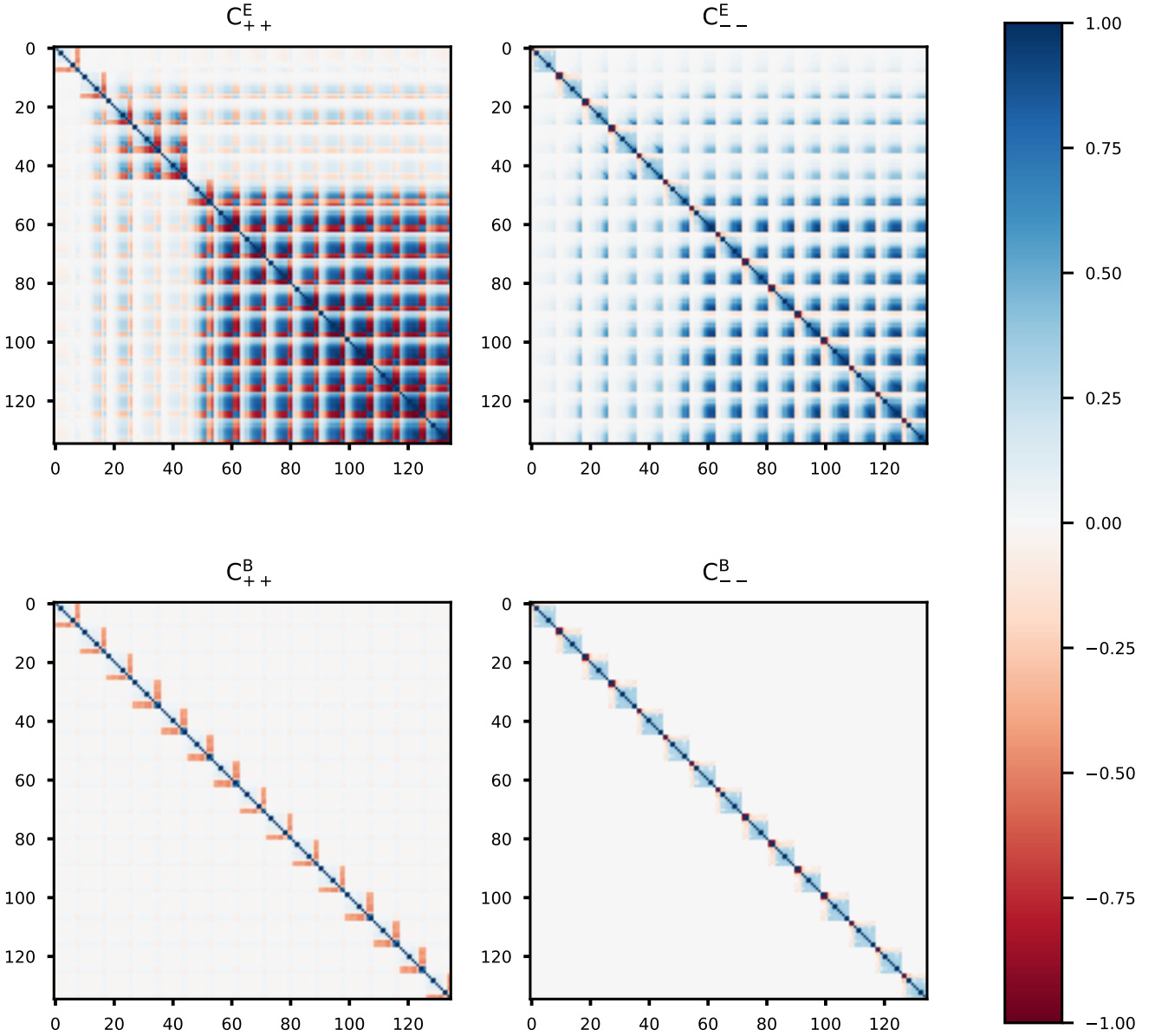


Fig. 8. Correlation coefficients for pure-mode correlation functions. These are shown for the auto-correlations of ξ_+^E (top left), ξ_-^E (top right), ξ_+^B (bottom left) and ξ_-^B (bottom right). The covariance matrices are calculated for 9 θ -bins and 5 redshift bins, resulting in 15 distinct pairs of redshifts. The top left corner of each panel shows the correlation coefficients for the lowest redshift bins.

either made a significant contribution to the data products, or to the scientific analysis.

References

- Aihara, H., Arimoto, N., Armstrong, R., et al. 2018, *PASJ*, 70, S4
- Albrecht, A., Bernstein, G., Cahn, R., et al. 2006, *astro-ph/060959*
- Asgari, M. & Heymans, C. 2019, *MNRAS*, 484, L59
- Asgari, M., Heymans, C., Blake, C., et al. 2017, *MNRAS*, 464, 1676
- Asgari, M., Heymans, C., Hildebrandt, H., et al. 2019, *A&A*, 624, A134
- Asgari, M., Lin, C.-A., Joachimi, B., et al. 2021, *A&A*, 645, A104
- Asgari, M. & Schneider, P. 2015, *A&A*, 578, A50
- Asgari, M., Schneider, P., & Simon, P. 2012, *A&A*, 542, A122
- Asgari, M., Tröster, T., Heymans, C., et al. 2020, *A&A*, 634, A127
- Becker, M. R. 2013, *MNRAS*, 435, 1547
- Becker, M. R. & Rozo, E. 2016, *MNRAS*, 457, 304
- Blandford, R. D., Saust, A. B., Brainerd, T. G., & Villumsen, J. V. 1991, *MNRAS*, 251, 600
- Blazek, J. A., MacCrann, N., Troxel, M. A., & Fang, X. 2019, *Phys. Rev. D*, 100, 103506
- Bridle, S. & King, L. 2007, *New Journal of Physics*, 9, 444
- Bunn, E. F. 2011, *Phys. Rev. D*, 83, 083003
- Crittenden, R. G., Natarajan, P., Pen, U.-L., & Theuns, T. 2002, *ApJ*, 568, 20
- DES Collaboration, Abbott, T. M. C., Aguena, M., et al. 2021, *arXiv e-prints*, arXiv:2105.13549
- Deshpande, A. C., Kitching, T. D., Cardone, V. F., et al. 2020, *A&A*, 636, A95
- Drlica-Wagner, A., Sevilla-Noarbe, I., Rykoff, E. S., et al. 2018, *ApJS*, 235, 33
- Edge, A., Sutherland, W., Kuijken, K., et al. 2013, *The Messenger*, 154, 32
- Erben, T., Hildebrandt, H., Miller, L., et al. 2013, *MNRAS*, 433, 2545
- Gatti, M., Sheldon, E., Amon, A., et al. 2021, *MNRAS*, 504, 4312
- Giahi-Saravani, A. & Schäfer, B. M. 2014, *MNRAS*, 437, 1847
- Giblin, B., Heymans, C., Asgari, M., et al. 2021, *A&A*, 645, A105
- Harnois-Déraps, J., Amon, A., Choi, A., et al. 2018, *MNRAS*, 481, 1337
- Heydenreich, S., Schneider, P., Hildebrandt, H., et al. 2020, *A&A*, 634, A104
- Heymans, C., Grocutt, E., Heavens, A., et al. 2013, *MNRAS*, 432, 2433
- Heymans, C., Tröster, T., Asgari, M., et al. 2021, *A&A*, 646, A140
- Heymans, C., Van Waerbeke, L., Miller, L., et al. 2012, *MNRAS*, 427, 146
- Heymans, C., White, M., Heavens, A., Vale, C., & van Waerbeke, L. 2006, *MNRAS*, 371, 750

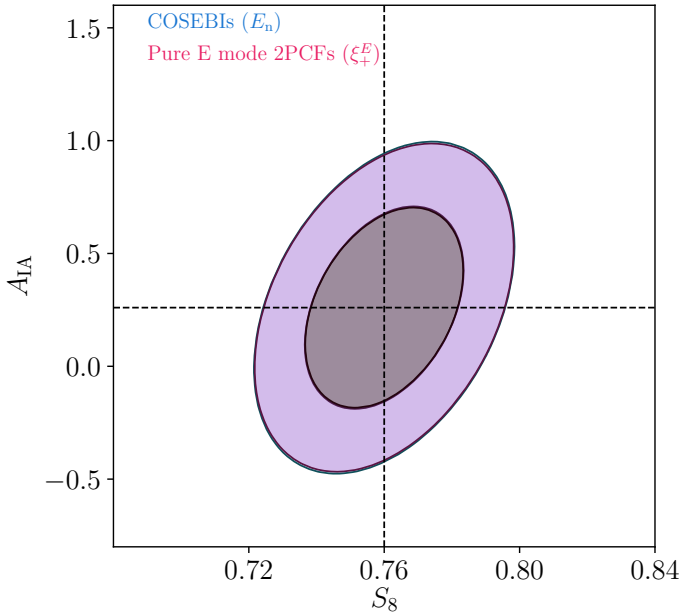


Fig. 9. Fisher matrix forecast for KiDS-1000. The SEK COSEBIs (blue) are compared with ξ_+^E (pink), showing that they contain the same level of information about the model parameters, S_8 and A_{1A} . All other parameters, listed in Table 1, are fixed to their fiducial values. The fact that one sees only one ellipse is because both methods give the same Fisher ellipses, and thus lie on top of each other, as expected. This figure is made with CHAINCONSUMER (Hinton 2016).

Hilbert, S., Hartlap, J., White, S. D. M., & Schneider, P. 2009, *A&A*, 499, 31
Hilbert, S., Xu, D., Schneider, P., et al. 2017, *MNRAS*, 468, 790
Hildebrandt, H., van den Busch, J. L., Wright, A. H., et al. 2021, *A&A*, 647, A124
Hildebrandt, H., Viola, M., Heymans, C., et al. 2017, *MNRAS*, 465, 1454
Hinton, S. R. 2016, *The Journal of Open Source Software*, 1, 00045
Hirata, C. M. & Seljak, U. 2004, *Phys. Rev. D*, 70, 063526
Joachimi, B., Cacciato, M., Kitching, T. D., et al. 2015, *Space Sci. Rev.*, 193, 1
Joachimi, B., Lin, C. A., Asgari, M., et al. 2021, *A&A*, 646, A129
Joachimi, B., Semboloni, E., Hilbert, S., et al. 2013, *MNRAS*, 436, 819
Kaiser, N. 1992, *ApJ*, 388, 272
Kaiser, N. 1998, *ApJ*, 498, 26
Kilbinger, M. 2018, *arXiv e-prints*, arXiv:1807.08249
Kilbinger, M., Schneider, P., & Eifler, T. 2006, *A&A*, 457, 15
Kitching, T. D., Paykari, P., Hoekstra, H., & Cropper, M. 2019, *The Open Journal of Astrophysics*, 2, 5
Krause, E. & Hirata, C. M. 2010, *A&A*, 523, A28
Kuijken, K., Heymans, C., Dvornik, A., et al. 2019, *A&A*, 625, A2
Kuijken, K., Heymans, C., Hildebrandt, H., et al. 2015, *MNRAS*, 454, 3500
Lewis, A., Challinor, A., & Lasenby, A. 2000, *ApJ*, 538, 473
LoVerde, M. & Afshordi, N. 2008, *Phys. Rev. D*, 78, 123506
Mandelbaum, R. 2018, *ARA&A*, 56, 393
Mead, A. J., Peacock, J. A., Heymans, C., Joudaki, S., & Heavens, A. F. 2015, *MNRAS*, 454, 1958
Peacock, J. A., Schneider, P., Efstathiou, G., et al. 2006, *ESA-ESO Working Group on “Fundamental Cosmology”*, Tech. rep.
Schneider, P. 1996, *MNRAS*, 283, 837
Schneider, P., Eifler, T., & Krause, E. 2010, *A&A*, 520, A116
Schneider, P. & Kilbinger, M. 2007, *A&A*, 462, 841
Schneider, P. & Seitz, C. 1995, *A&A*, 294, 411
Schneider, P., van Waerbeke, L., Jain, B., & Kruse, G. 1998, *MNRAS*, 296, 873
Schneider, P., van Waerbeke, L., & Mellier, Y. 2002, *A&A*, 389, 729
Sevilla-Noarbe, I., Bechtol, K., Carrasco Kind, M., et al. 2021, *ApJS*, 254, 24
Shapiro, C. 2009, *ApJ*, 696, 775
Troxel, M. A. & Ishak, M. 2015, *Phys. Rep.*, 558, 1
Vale, C., Hoekstra, H., van Waerbeke, L., & White, M. 2004, *ApJ*, 613, L1
White, M. 2005, *Astroparticle Physics*, 23, 349
Wolfram, S. 1991, *Mathematica: a system for doing mathematics by computer*, ed. Wolfram, S.
Zuntz, J., Paterno, M., Jennings, E., et al. 2015, *Astronomy and Computing*, 12, 45
Zuntz, J., Sheldon, E., Samuroff, S., et al. 2018, *MNRAS*, 481, 1149

Appendix A: Shear fields from ambiguous modes

In this appendix, we will consider ambiguous modes of the shear field in more detail. This will be done in different ways. First, we will give several examples of shear fields which can not uniquely be assigned to either E-mode or B-mode shear. We then show that a statistical ensemble of such shear fields give rise to the ambiguous modes in the shear two-point correlation functions. Finally, we show that ambiguous modes in the shear correlation functions can be caused by various combinations of E- and B-mode power spectra.

Appendix A.1: Ambiguous shear fields

Following Crittenden et al. (2002) and Schneider et al. (2002), we formally describe a general shear field by a superposition of E- and B-modes, by defining the complex deflection potential $\psi(\theta) = \psi^E(\theta) + i\psi^B(\theta)$, where $\psi^{E/B}$ are real functions. The corresponding convergence is then obtained from the Poisson equation, $\kappa(\theta) = \kappa^E(\theta) + i\kappa^B(\theta) = (1/2)\nabla^2\psi(\theta)$. The shear field is given by

$$\gamma = \gamma_1 + i\gamma_2 = \left[\frac{\psi_{,11}^E - \psi_{,22}^E}{2} - \psi_{,12}^B \right] + i \left[\psi_{,12}^E + \frac{\psi_{,11}^B - \psi_{,22}^B}{2} \right], \quad (\text{A.1})$$

where subscripts following a comma denote partial derivatives with respect to θ_i . We consider the following combinations of second derivatives of the shear,

$$\begin{aligned} C_c &:= \gamma_{2,11} - \gamma_{2,22} - 2\gamma_{1,12} = \frac{1}{2}(\psi_{,1111}^B + \psi_{,2222}^B) + \psi_{,1122}^B; \\ C_g &:= \gamma_{1,11} - \gamma_{1,22} + 2\gamma_{2,12} = \frac{1}{2}(\psi_{,1111}^E + \psi_{,2222}^E) + \psi_{,1122}^E. \end{aligned} \quad (\text{A.2})$$

Thus we see that a shear field which does not contain a B-mode component satisfies $C_c \equiv 0$, whereas one that has no E-mode contribution satisfies $C_g \equiv 0$. In the following, we will provide examples for shear fields for which $C_g \equiv 0 \equiv C_c$, and thus result either from an E- or a B-mode deflection potential.

The first example is one where the deflection potential is a polynomial of order 3. Since constant and linear terms in ψ do not cause any shear, we write

$$\begin{aligned} \psi^{E/B} &= a_{11}^{E/B}\theta_1^2 + a_{12}^{E/B}\theta_1\theta_2 + a_{22}^{E/B}\theta_2^2 \\ &\quad + b_{111}^{E/B}\theta_1^3 + b_{112}^{E/B}\theta_1^2\theta_2 + b_{122}^{E/B}\theta_1\theta_2^2 + b_{222}^{E/B}\theta_2^3. \end{aligned} \quad (\text{A.3})$$

This yields the linear shear field

$$\begin{aligned} \gamma_1 &= a_{11}^E - a_{22}^E - a_{12}^B + (3b_{111}^E - b_{122}^E - 2b_{112}^B)\theta_1 \\ &\quad + (b_{112}^E - 3b_{222}^E - 2b_{122}^B)\theta_2 \\ \gamma_2 &= a_{12}^E + a_{11}^B - a_{22}^B + (2b_{112}^E + 3b_{111}^B - b_{122}^B)\theta_1 \\ &\quad + (2b_{122}^E + b_{112}^B - 3b_{222}^B)\theta_2. \end{aligned} \quad (\text{A.4})$$

It is obvious that such a linear shear field can be equally obtained from E-mode and B-mode deflection potentials, and thus such a shear field corresponds to an ambiguous mode. Obviously, $C_g \equiv 0 \equiv C_c$ for such a field.

A less trivial example is obtained by considering axisymmetric shear fields of the form

$$\gamma(\theta) = -F(|\theta|^2) \frac{\theta}{\theta^*}, \quad (\text{A.5})$$

where we here use complex notation for a vector θ , i.e., $\theta = \theta_1 + i\theta_2$, and the asterisk denotes complex conjugation. The term $\theta/\theta^* = e^{2i\varphi}$, where φ is the polar angle of θ , is just a phase factor. Such a shear field is tangential to the origin at every point, and can be generated by an axi-symmetric mass distribution κ^E or, equivalently, an axi-symmetric deflection potential ψ^E . From Eq. (A.2) we find that $C_c(\theta) \equiv 0$ for this shear field, independent of the function F . For C_g , we find

$$C_g(\theta) = -4 \left[2F'(|\theta|^2) + |\theta|^2 F''(|\theta|^2) \right], \quad (\text{A.6})$$

which is non-zero in general. However, for $F(X) = \text{const.}$ or $F(X) \propto X^{-1}$, C_g also vanishes. We consider the latter case first: it corresponds to

$$\gamma(\theta) = -\frac{1}{|\theta|^2} \frac{\theta}{\theta^*} = -\frac{1}{\theta^{*2}}, \quad (\text{A.7})$$

the shear field of a point mass. Curiously, we can also get the same shear field from a B-mode potential. Indeed, we let

$$\psi^E = \frac{1-f}{2} \ln(|\theta|^2); \quad \psi^B = -f \arctan(\theta_2/\theta_1), \quad (\text{A.8})$$

then we get

$$\gamma(\theta) = -\frac{\theta_1^2 - \theta_2^2 + 2i\theta_1\theta_2}{|\theta|^4}, \quad (\text{A.9})$$

in agreement with Eq. (A.7), for any value of f . This indeed is a curious result, stating that a pure tangential shear field – the ‘classical’ case of an E-mode field – can be obtained from a B-mode potential. Putting this in different words: If we take the tangential shear field (A.7) and rotate the shear at every position by 45 degree (equivalent to multiplying the shear by a factor i), then we get the classical case of a B-mode shear field. However, this rotated field can be obtained from a pure E-mode potential $\psi^E = -\arctan(\theta_2/\theta_1)$. We should point out, though, that the $\arctan(\theta_2/\theta_1)$ is not defined on the θ_2 -axis where it jumps from $-\pi/2$ to $\pi/2$, and thus the rosetta-like shear field cannot be obtained from a globally-defined E-mode potential (or convergence). But if one considers the shear field on any finite region not crossing the θ_2 -axis, one cannot tell whether the shear field (A.7) is due to an E- or a B-mode.⁷

Likewise, the shear field

$$\gamma(\theta) = -\frac{\theta}{\theta^*}, \quad (\text{A.10})$$

which is a tangential shear field with an amplitude independent of radius $|\theta|$, can be generated both by an E- and B-mode deflection potential: Letting

$$\psi^E = \frac{f-1}{2} |\theta|^2 \ln(|\theta|^2); \quad \psi^B = f |\theta|^2 \arctan(\theta_2/\theta_1), \quad (\text{A.11})$$

leads to the shear field (A.10), for any f .

⁷ Note that $\arctan(\theta_2/\theta_1) = \varphi$ for $-\pi/2 < \varphi < \pi/2$. Hence, we could replace the $\arctan(\theta_2/\theta_1)$ just by φ . In this case, the function would undergo only one discontinuity on a circle around the origin.

Appendix A.2: Shear correlation functions from ambiguous shear fields

We will now consider isotropic statistical ensembles of ambiguous shear fields and consider the resulting shear correlation functions. For that, we consider the shear on two points on the θ_1 -axis, at $\theta = (\pm\vartheta/2, 0)$, so that $\xi_+(\vartheta) = \langle \gamma(-\vartheta/2) \gamma^*(\vartheta/2) \rangle$ and $\xi_-(\vartheta) = \langle \gamma(-\vartheta/2) \gamma(\vartheta/2) \rangle$.⁸ Starting with the linear shear field, we consider an ensemble of such fields, and write the shear in complex notation as

$$\gamma(\theta) = G_2 + G_1\theta + G_3\theta^*, \quad (\text{A.12})$$

where due to the fact that the shear is a spin-2 field, the coefficients G_n are spin- n quantities which under a rotation of the coordinate frame, they transform as $G_n \rightarrow G_n e^{-in\varphi}$. Accordingly,

$$\begin{aligned} \gamma(-\vartheta/2) \gamma(\vartheta/2) &= G_2^2 - (G_1^2 + G_3^2 + 2G_1G_3)\vartheta^2/4, \\ \gamma(-\vartheta/2) \gamma^*(\vartheta/2) &= |G_2|^2 - (|G_1|^2 + |G_3|^2 + G_1G_3^* + G_1^*G_3)\vartheta^2/4 \\ &\quad + [G_2(G_1^* + G_3^*) - G_2^*(G_1 + G_3)]\vartheta/2. \end{aligned} \quad (\text{A.13})$$

If we now consider a statistical ensemble of such linear fields, we have to average over the coefficients. Statistical isotropy then implies that $\langle G_m G_n \rangle = 0 = \langle G_m G_n^* \rangle$ for $m \neq n$, as well $\langle G_n G_n \rangle = 0$, due to phase averaging over these spin $\neq 0$ quantities. Therefore,

$$\begin{aligned} \xi_+(\vartheta) &= \langle \gamma(-\vartheta/2) \gamma^*(\vartheta/2) \rangle = |G_2|^2 - (|G_1|^2 + |G_3|^2)\vartheta^2/4, \\ \xi_-(\vartheta) &= \langle \gamma(-\vartheta/2) \gamma(\vartheta/2) \rangle = 0, \end{aligned} \quad (\text{A.14})$$

which corresponds to the ambiguous modes discussed in Sect. A.1.

We next turn to the shear field caused by an ensemble of point masses. Specifically, we consider a circular region of radius Θ in which there are N point masses at locations θ_i and relative masses m_i , with mean mass $\langle m \rangle$. At the end we will consider the limit $\Theta \rightarrow \infty$, $N \rightarrow \infty$, such that the mean number density $\bar{n} = N/(\pi\Theta^2)$ is constant. The shear field then reads

$$\gamma(\theta) = \sum_{i=1}^N \left(\frac{m_i}{(\theta - \theta_i)^2} \right)^*. \quad (\text{A.15})$$

We assume the positions θ_i of the point masses to be random inside the circle. Therefore, the expectation value of the product $\gamma(-\vartheta/2) \gamma(\vartheta/2)$ is

$$\begin{aligned} \xi_-(\vartheta) &= \langle \gamma(-\vartheta/2) \gamma(\vartheta/2) \rangle = \left[\prod_{n=1}^N \frac{1}{\pi\Theta^2} \int_0^\Theta d|\theta_n| |\theta_n| \int_0^{2\pi} d\varphi_n \right] \\ &\quad \times \sum_{i,j=1}^N \left(\frac{m_i}{(\theta_i - \vartheta/2)^2} \frac{m_j}{(\theta_j + \vartheta/2)^2} \right)^*. \end{aligned} \quad (\text{A.16})$$

We now split the sum into terms $i \neq j$ and those with $i = j$. In the former case, each term of the sum depends only on two θ_n , and the rest integrate out to unity. Those off-diagonal terms yield

$$\sum_{i \neq j}^N \frac{m_i m_j}{(\pi\Theta^2)^2} I^*(\vartheta/2) I^*(-\vartheta/2), \quad (\text{A.17})$$

⁸ Note that the imaginary part of these correlators vanish due to parity invariance.

where

$$I(\vartheta/2) = \int_0^\Theta d\theta \int_0^{2\pi} d\varphi \frac{1}{(\theta e^{i\varphi} - \vartheta/2)^2}. \quad (\text{A.18})$$

We can now calculate the inner integral. For that, we let $u = e^{i\varphi}$, $d\varphi = -i du/u$, so the φ -integral becomes

$$\int_0^{2\pi} d\varphi \frac{1}{(\theta e^{i\varphi} - \vartheta/2)^2} = -i \oint \frac{du}{u} \frac{1}{(\theta u - \vartheta/2)^2}, \quad (\text{A.19})$$

where the integral extends over the unit circle. This integral was calculated in Schneider (1996) to yield

$$\frac{4\pi}{\vartheta^2} \left[2H\left(\frac{\vartheta}{2} - \theta\right) - \frac{\vartheta}{2} \delta_D\left(\theta - \frac{\vartheta}{2}\right) \right]. \quad (\text{A.20})$$

so that $I(\vartheta/2) = 0$ for $\Theta > \vartheta/2$. Thus, the off-diagonal terms in Eq. (A.16) do not contribute to ξ_- . In fact, $I(\theta)$ is the shear caused by a uniform disk of matter of radius Θ , and it is well known that such a disk causes no shear for $\Theta > \theta$.

This leaves us with the diagonal terms $i = j$,

$$\xi_-(\vartheta) = \frac{N \langle m^2 \rangle}{\pi \Theta^2} \int_0^\Theta d\theta \oint \frac{-i du}{u} \frac{1}{(\theta u - \vartheta/2)^2} \frac{1}{(\theta u + \vartheta/2)^2}. \quad (\text{A.21})$$

Employing the residue theorem, we note three poles at $u_1 = 0$, $u_2 = \vartheta/(2\theta)$ and $u_3 = -\vartheta/(2\theta)$, with $\text{Res}(u_1) = 16/\vartheta^4$, $\text{Res}(u_2) = \text{Res}(u_3) = -8/\vartheta^4$. The latter two poles lie inside the unit circle for $\theta > \vartheta/2$, and for this case, the contour integral vanishes. Thus we find

$$\xi_-(\vartheta) = \bar{n} \langle m^2 \rangle \frac{4\pi}{\vartheta^2}, \quad (\text{A.22})$$

corresponding to one of the ambiguous modes discussed in Sect. A.1. Repeating the calculations for the correlation $\xi_+(\vartheta)$, we find that the non-diagonal terms in the double sum vanish as well, and we are left with

$$\xi_+(\vartheta) = \frac{N \langle m^2 \rangle}{\pi \Theta^2} \int_0^\Theta d\theta \oint \frac{-i du}{u} \frac{1}{(\theta u - \vartheta/2)^2} \frac{1}{(\theta u + \vartheta/2)^2}. \quad (\text{A.23})$$

The integrand in the contour integral has poles at $u_1 = \vartheta/(2\theta)$ and $u_2 = -\vartheta/(2\theta)$, and the corresponding residue are $\text{Res}(u_1) = -16(\vartheta^2 - 4\theta^2)/(\vartheta^2 + 4\theta^2)^3$ and $\text{Res}(u_2) = 16(\vartheta^2 - 4\theta^2)/(\vartheta^2 + 4\theta^2)^3$. The former (latter) pole is inside the unit circle for $\theta > \vartheta/2$ ($\theta < \vartheta/2$). Performing the θ -integral then yields $\xi_+(\vartheta) = 0$.

In fact, this result could have been anticipated: The convergence power spectrum for a random field of point masses is a constant, and the correlation function of the convergence vanishes for any finite separation. But the shear correlation function ξ_+ is identical to the convergence correlation, so that $\xi_+(\vartheta) = 0$ for $\vartheta > 0$. Furthermore, for a constant power spectrum, the second of Eqs. (69) shows that $\xi_-(\vartheta) \propto \vartheta^{-2}$. We also note that the first of Eqs. (61) implies that $\xi_-(\vartheta) \propto \vartheta^{-2}$ yields $\xi_+(\vartheta) = 0$.

We have been unable to find an analogous example of a shear field which can be obtained from a deflection potential and which yields a $\xi_-(\vartheta) \propto \vartheta^{-4}$ correlation. However, if we drop the requirement that the shear field can be obtained from a potential – for example, the shear field is due to some systematics

unrelated to the lensing effect – then one can construct such examples. If we consider the spin-3 field

$$\gamma(\theta) = F(|\theta|^2) \theta^3, \quad (\text{A.24})$$

then we find that $C_c \equiv 0 \equiv C_g$ if $F(X)$ satisfies the differential equation $X^2 F'' + 6X F' + 6F = 0$. The two independent solutions, $F \propto X^{-2}$ and $F \propto X^{-3}$, then lead to shear fields of the form $\gamma(\theta) \propto \theta^3/|\theta|^4$ and $\gamma(\theta) \propto \theta^3/|\theta|^6$. Choosing the latter one of those and constructing a random field with it, in the same way as we did above for the point masses, we find indeed that $\xi_-(\vartheta) \propto \vartheta^{-4}$.

Appendix A.3: Ambiguous modes in ξ_\pm and their relation to power spectra

We will here consider the relation between shear correlation function and the underlying power spectra, and provide examples of correlations functions that can be derived equally well from an E- or B-mode power spectrum, or a linear combination of both.

We start by noting that the relation between the correlation functions and the E- and B-mode power spectra, $P_E(\ell)$ and $P_B(\ell)$, respectively, is given by Eq. (69). If the correlation functions are known for all ϑ , one can invert these relations and get a unique decomposition into E- and B-modes,

$$\begin{aligned} P_E(\ell) &= \pi \int_0^\infty d\vartheta \vartheta [\xi_+(\vartheta) J_0(\ell\vartheta) + \xi_-(\vartheta) J_4(\ell\vartheta)] ; \\ P_B(\ell) &= \pi \int_0^\infty d\vartheta \vartheta [\xi_+(\vartheta) J_0(\ell\vartheta) - \xi_-(\vartheta) J_4(\ell\vartheta)] , \end{aligned} \quad (\text{A.25})$$

but on a finite interval of separations, this decomposition is not possible. As an example, consider the power spectrum⁹

$$P_0(\ell) = \frac{2\pi\vartheta_2}{\ell^2\vartheta_0^2} \left[\ell(\vartheta_0^2 \xi_0 + \vartheta_2^2 \xi_2) J_1(\ell\vartheta_2) - 2\vartheta_2 \xi_2 J_2(\ell\vartheta_2) \right], \quad (\text{A.26})$$

where $\vartheta_2 > \vartheta_{\max}$, and ϑ_0 is a fiducial angular scale, and let the E- and B-mode power spectra be $P_E(\ell) = f P_0(\ell)$, $P_B(\ell) = (1 - f) P_0(\ell)$. Then we find from Eq. (69) that

$$\xi_+(\vartheta) = \xi_0 + \xi_2 \left(\frac{\vartheta}{\vartheta_0} \right)^2 ; \quad \xi_-(\vartheta) = 0 \quad (\text{A.27})$$

for $\vartheta < \vartheta_2$, and thus for $\vartheta \leq \vartheta_{\max}$, valid for any value of f . Hence, we can obtain the pair of correlation functions (A.27) for any distribution of power on the E- and B-mode power spectra. Therefore, we have the two ambiguous modes $\xi_+ = \text{const.}$ and $\xi_+ \propto \vartheta^2$. We note that these modes are ambiguous only on a finite interval. For $\vartheta > \vartheta_2$, $\xi_+ = 0$, but $\xi_- \neq 0$, and in particular, $\xi_- \propto (2f - 1)$. Hence, if we had information about ξ_\pm on all scales, we could determine the parameter f , and the mode assignment would be unique.

Similarly, we consider the power spectrum

$$P_0(\ell) = \frac{2\pi\vartheta_0^2}{\ell^2\vartheta_1^3} \left[2\xi_{-2}\vartheta_1 J_2(\ell\vartheta_1) + \ell(\xi_{-2}\vartheta_1^2 + \xi_{-4}\vartheta_0^2) J_3(\ell\vartheta_1) \right], \quad (\text{A.28})$$

⁹ We ignore the fact that P_0 can be negative; instead, we may assume that P_0 is an additive contribution to a total power spectrum which is positive for all ℓ .

where $\vartheta_1 < \vartheta_{\min}$. We now distribute this power as $P_E(\ell) = (1+f)P_0(\ell)$, $P_B(\ell) = fP_0(\ell)$ over E- and B-modes, and then find from Eq. (69) that

$$\xi_+(\vartheta) = 0; \quad \xi_-(\vartheta) = \xi_{-2} \left(\frac{\vartheta}{\vartheta_0} \right)^{-2} + \xi_{-4} \left(\frac{\vartheta}{\vartheta_0} \right)^{-4}, \quad (\text{A.29})$$

valid for $\vartheta > \vartheta_1$, and thus for $\vartheta \geq \vartheta_{\min}$. We note that this pair of correlation functions are independent of f , and thus valid for any distribution of the power P_0 over E- and B-modes. Hence, this is a second pair of ambiguous modes, namely $\xi_+ = 0$, and $\xi_- \propto \vartheta^{-2}$ and $\xi_- \propto \vartheta^{-4}$. Whereas $\xi_-(\vartheta) = 0$ for $\vartheta < \vartheta_1$, $\xi_+(\vartheta) \neq 0$ for smaller ϑ , and in particular it is proportional to $(1+2f)$. Thus again, these modes are ambiguous only on a finite interval.

For the more general case, let us assume that the correlation functions $\xi_+(\vartheta) = \xi_+^0(\vartheta) + \Delta\xi_+(\vartheta)$, $\xi_-(\vartheta) = \xi_-^0(\vartheta) + \Delta\xi_-(\vartheta)$ are written as a sum of two terms, where the ones with ‘0’ superscript do not yield any ambiguous modes $E_{a,b}^0 = 0 = B_{a,b}^0$. On the other hand, we assume that $\Delta\xi_+(\vartheta)$ is purely ambiguous, i.e., of the form $\Delta\xi_+(\vartheta) = \xi_0 + \xi_2(\vartheta/\vartheta_0)^2$ on the finite interval $\vartheta_{\min} \leq \vartheta \leq \vartheta_{\max}$, but has an arbitrary functional form for larger and smaller separations. The coefficients $\xi_{0,2}$ are directly related to the $E_{a,b} + B_{a,b}$ defined above. From Eq. (A.25), we then find

$$P_0 := \Delta P_E(\ell) + \Delta P_B(\ell) = 2\pi \int_0^\infty d\vartheta \vartheta J_0(\ell\vartheta) \Delta\xi_+(\vartheta). \quad (\text{A.30})$$

We again distribute the power over modes in the form $\Delta P_E(\ell) = fP_0(\ell)$, $\Delta P_B(\ell) = (1-f)P_0(\ell)$, and then calculate $\Delta\xi_-(\vartheta)$ on the finite interval,

$$\begin{aligned} \Delta\xi_-(\vartheta) &= (2f-1) \int_0^\infty d\ell \ell J_4(\ell\vartheta) \int_0^\infty d\theta \theta J_0(\ell\theta) \Delta\xi_+(\theta) \\ &= (2f-1) \left\{ \Delta\xi_+(\vartheta) + \int_0^{\vartheta_{\min}} d\theta \theta \Delta\xi_+(\theta) \left(\frac{4}{\vartheta^2} - \frac{12\vartheta^2}{\vartheta^4} \right) \right. \\ &\quad \left. + \int_{\vartheta_{\min}}^\vartheta d\theta \theta \left[\xi_0 + \xi_2 \left(\frac{\vartheta}{\vartheta_0} \right)^2 \right] \left(\frac{4}{\vartheta^2} - \frac{12\vartheta^2}{\vartheta^4} \right) \right\} \quad (\text{A.31}) \\ &= (2f-1) \left\{ \frac{1}{\vartheta^2} \left[4 \int_0^{\vartheta_{\min}} d\theta \theta \Delta\xi_+(\theta) - 2\vartheta_{\min}^2 \xi_0 - \frac{\vartheta_{\min}^4}{\vartheta_0^2} \xi_2 \right] \right. \\ &\quad \left. + \frac{1}{\vartheta^4} \left[12 \int_0^{\vartheta_{\min}} d\theta \theta^3 \Delta\xi_+(\theta) + 3\vartheta_{\min}^4 \xi_0 + \frac{2\vartheta_{\min}^6}{\vartheta_0^2} \xi_2 \right] \right\}, \end{aligned}$$

where we made use of the relation

$$\int_0^\infty d\ell \ell J_0(\ell\vartheta) J_4(\ell\theta) = \frac{1}{\vartheta} \delta_D(\vartheta - \theta) + \left(\frac{4}{\vartheta^2} - \frac{12\vartheta^2}{\vartheta^4} \right) H(\theta - \vartheta),$$

where δ_D and H denote the Dirac delta ‘function’ and the Heaviside step function, respectively. We see that $\Delta\xi_-(\vartheta)$ only contains ambiguous modes inside the finite interval, and that the amplitudes of these depend on the integral of $\Delta\xi_+$ over scales below ϑ_{\min} , i.e., assumed to be unmeasured. Because of this, the fraction f of B-mode power attributed to the $\Delta\xi_\pm$ can not be determined. We can go through the analogous exercise to fix $\Delta\xi_-$ and calculate $\Delta\xi_+$, which then only contains ambiguous modes with an amplitude that depends on f and moments of ξ_- taken over scales larger than ϑ_{\max} .

Appendix B: A new set of COSEBIs

The $\mu = n$ coefficients in Eq. (17) define the COSEBIs. These COSEBIs depend on the choice of the weight functions $T_{\pm n}(\vartheta)$.

We point out that the $T_{\pm n}(\vartheta)$ used in this paper differ from those in SEK in their dimensions: whereas in SEK, these filter functions were chosen to be dimensionless, we choose them here to have dimension $(\text{angle})^{-2}$, as can be seen from Eq. (6). Correspondingly, the COSEBIs defined here are dimensionless, whereas they have dimension $(\text{angle})^2$ in SEK. We think the current choice is more natural than the earlier one.

Furthermore, our orthonormality relation (6) differs from that of SEK through the factor ϑ in the integral. This new definition allowed us to show that the $T_{-n}(\vartheta)$ also form an orthonormal basis, which they do not with the orthonormality relation used in SEK.

In SEK, we constructed two sets of function $T_{\pm n}(\vartheta)$, one being polynomials in ϑ , the other being polynomials in $\ln(\vartheta)$, termed linear and logarithmic COSEBIs, respectively. The latter were shown to be more convenient, in that fewer COSEBI modes are needed to extract the full cosmological information contained in mode-separable correlation functions.

Appendix B.1: Linear COSEBIs

We consider the case of polynomial COSEBIs first, for which we transform the interval $\vartheta_{\min} \leq \vartheta \leq \vartheta_{\max}$ onto the interval $-1 \leq x \leq 1$ via

$$\vartheta = \bar{\vartheta}(1+Bx). \quad (\text{B.1})$$

We then set $T_{\pm n}(\vartheta) = \bar{\vartheta}^{-2} t_{\pm n}(x)$. Since $d\vartheta = B\bar{\vartheta} dx$, we then see from Eqs. (6) and (14) that the $t_{\pm n}(x)$ obey the orthonormality relations

$$\int_{-1}^1 dx (1+Bx) t_{\pm m}(x) t_{\pm n}(x) = \delta_{mn}. \quad (\text{B.2})$$

This equation also motivates the prefactor in the orthonormality relation (6). Furthermore, the constraints (4) are translated into

$$\int_{-1}^1 dx (1+Bx) t_{+n}(x) = 0 = \int_{-1}^1 dx (1+Bx)^3 t_{+n}(x). \quad (\text{B.3})$$

The functions $T_{-n}(\vartheta) = \bar{\vartheta}^{-2} t_{-n}(x)$ are then calculated from

$$\begin{aligned} t_{-n}(x) &= t_{+n}(x) + \frac{4B}{(1+Bx)^2} \int_{-1}^x dy (1+By) t_{+n}(y) \\ &\quad - \frac{12B}{(1+Bx)^4} \int_{-1}^x dy (1+By)^3 t_{+n}(y). \end{aligned} \quad (\text{B.4})$$

We constructed a set of polynomial functions $t_{+n}(x)$ obeying the orthonormality relation (B.2) and the constraints (B.3), where $t_{+n}(x)$ is a polynomial of $(n+1)$ -th order, given by

$$\begin{aligned} t_{+1}(x) &= \frac{(5-B^2)P_2(x) - 3BP_1(x) + B^2P_0(x)}{\sqrt{10-6B^2}} \\ t_{+n}(x) &= \left[2(n+2)B P_{n+1} \left(\frac{1}{B} \right) P_{n+2} \left(\frac{1}{B} \right) \right]^{-1/2} \\ &\quad \times \sum_{k=0}^{n+1} (-1)^k (2k+1) P_k \left(\frac{1}{B} \right) P_k(x) \quad \text{for } n \geq 2. \end{aligned} \quad (\text{B.5})$$

The sign of the $t_{+n}(x)$ has been chosen such that $t_{+n}(-1) > 0$, implying $T_{+n}(\vartheta_{\min}) > 0$. In order to show the validity of this

result, we first consider, for $n \geq 2$, the expression

$$\begin{aligned} (1+Bx) \sum_{k=0}^{n+1} (-1)^k (2k+1) P_k \left(\frac{1}{B} \right) P_k(x) \\ = B \sum_{k=0}^{n+1} (-1)^k \left\{ \frac{2k+1}{B} P_k \left(\frac{1}{B} \right) P_k(x) \right. \\ \left. + P_k \left(\frac{1}{B} \right) [(k+1)P_{k+1}(x) + kP_{k-1}(x)] \right\}, \end{aligned} \quad (\text{B.6})$$

where we used the recursion relation for Legendre polynomials, P_k . Changing the summation index for the last two terms as $k \rightarrow k \pm 1$ and applying the recursion relation for Legendre polynomials again, this time for the $P_k(1/B)$, we see that only two terms survive, and we obtain

$$\begin{aligned} (1+Bx) \sum_{k=0}^{n+1} (-1)^k (2k+1) P_k \left(\frac{1}{B} \right) P_k(x) \\ = (-1)^{n+1} (n+2) B \left[P_{n+1} \left(\frac{1}{B} \right) P_{n+2}(x) + P_{n+2} \left(\frac{1}{B} \right) P_{n+1}(x) \right]. \end{aligned} \quad (\text{B.7})$$

Therefore we find that, for $n \geq 2$,

$$\begin{aligned} (1+Bx) t_{+n}(x) = (-1)^{n+1} \sqrt{\frac{(n+2)B}{2P_{n+1}(1/B)P_{n+2}(1/B)}} \\ \times \left[P_{n+1} \left(\frac{1}{B} \right) P_{n+2}(x) + P_{n+2} \left(\frac{1}{B} \right) P_{n+1}(x) \right]. \end{aligned} \quad (\text{B.8})$$

Using the orthogonality relation of the Legendre polynomials, it is then straightforward to show that the orthonormality relation (B.2) is satisfied for $m, n \geq 2$. Furthermore, since $(1+Bx)t_{+n}$ for $n \geq 2$ contains no term $P_k(x)$ with $k \leq 2$, the orthogonality relation is clearly valid for $m = 1, n \geq 2$. Finally, it is easy to see that the conditions (B.3) are satisfied for $n \geq 2$, and for $n = 1$, it can be shown from straightforward integration. Hence, the system (B.5) forms the set of polynomial weight functions we were looking for.

It should be stressed that these functions are easy to calculate: for a given survey set-up, one needs to calculate the $P_k(1/B)$ only once, and the $P_n(x)$ are easily obtainable from the recursion relation of the Legendre polynomials. Whereas it is possible in principle to obtain explicit expressions for the corresponding functions $t_{-n}(x)$, this may not be needed: since the calculation of COSEBIs requires the calculation of the ξ_{\pm} and the T_{-n} at a large number of ϑ -values (see Asgari & Schneider 2015), it is probably computationally more efficient to evaluate the integrals in Eq. (B.4) using very small increments in the upper bound x .

Appendix B.2: Logarithmic COSEBIs

The roots of the polynomial weight functions $T_{+n}(\vartheta)$ are fairly uniformly distributed over the interval $\vartheta_{\min} < \vartheta < \vartheta_{\max}$. The shear correlation functions $\xi_{\pm}(\vartheta)$ vary more strongly for smaller ϑ than for larger ϑ , and therefore are expected to contain more (cosmological) information on these smaller scales. Therefore, it is useful to consider a set of weight functions $T_{+n}(\vartheta)$ which also show more structure on smaller scales, as done before in SEK. We let

$$T_{+n}(\vartheta) = \frac{1}{\vartheta^2} t_{+n} \left(\ln \frac{\vartheta}{\vartheta_{\min}} \right), \quad (\text{B.9})$$

so that the functions $t_{+n}(z)$ are defined for $0 \leq z \leq \ln(\vartheta_{\max}/\vartheta_{\min}) = z_m$. The constraints (4) and the orthonormality relation (6) then read in terms of the t_{+n} :

$$\begin{aligned} \int_0^{z_m} dz e^{2z} t_{+n}(z) &= 0 \\ \int_0^{z_m} dz e^{4z} t_{+n}(z) &= 0 \\ \int_0^{z_m} dz e^{2z} t_{+n}(z) t_{+m}(z) &= \frac{B\vartheta^2}{\vartheta_{\min}^2} \delta_{mn}. \end{aligned} \quad (\text{B.10})$$

We now choose the $t_{+n}(z)$ to be polynomials of order $n+1$, and write them in the form

$$t_{+n}(z) = \sum_{k=0}^{n+1} c_{nk} z^k. \quad (\text{B.11})$$

The equations (B.10) then lead to a linear system of equations for the coefficients c_{nk} , as was shown in SEK. Indeed, this system is very similar to the corresponding one in SEK, and differs only in the definition of the orthonormality relation for the T_{+n} . Hence, we refer the reader to SEK for details of the method how the solution for the c_{nk} is obtained. As was mentioned there, one needs the c_{nk} to have very high numerical precision, in particular for large values of $\vartheta_{\max}/\vartheta_{\min}$. However, if we write the polynomials in the form

$$t_{+n}(z) = N_n \prod_{i=1}^{n+1} (z - r_{ni}), \quad (\text{B.12})$$

then a moderate precision for the roots r_{ni} is sufficient. As an example, for $\vartheta_{\max}/\vartheta_{\min} = 400$ and eight significant digits of the r_{ni} , the orthonormality relations for the first 20 T_{+n} are satisfied to better than 10^{-18} . In Fig. B.1, we display a Mathematica (Wolfram 1991) program which calculates the roots r_{ni} .

An expression for the corresponding function $T_{-n}(\vartheta) = t_{-n}[\ln(\vartheta/\vartheta_{\min})]/\vartheta^2$ can then be calculated from Eq. (3), yielding

$$t_{-n}(z) = t_{+n}(z) + \int_0^z dy t_{+n}(y) [4e^{2(y-z)} - 12e^{4(y-z)}]. \quad (\text{B.13})$$

Hence, the t_{-n} can be easily calculated as numerical integrals over the t_{+n} in the form (B.12).

The COSEBIs are related to the underlying power spectrum by the integral

$$E_n = \int_0^\infty \frac{d\ell}{2\pi} P_E(\ell) W_n(\ell), \quad (\text{B.14})$$

where the weight function W_n is given by

$$W_n(\ell) = \int_{\vartheta_{\min}}^{\vartheta_{\max}} d\vartheta T_{+n}(\vartheta) J_0(\vartheta\ell). \quad (\text{B.15})$$

These weight functions thus describe the sensitivity of the COSEBIs to the power spectrum. As an example, we plot in Fig. B.2 the function $W_5(\ell)$ and compare it to the corresponding one of the COSEBIs defined in SEK, in both cases for the logarithmic weight functions. As can be seen, the ‘new’ W_5 is significant non-zero over a somewhat broader range in ℓ . It is this feature that makes the new COSEBIs less correlated than the old ones, as shown in Fig. 7. On the other hand, the wider ℓ -range may lead to an increase of the sensitivity of the COSEBIs to different baryonic feedback effects, compared to that of the SEK COSEBIs (see Asgari et al. 2020), which shall be explored in future work.

```

Nmax=20; tmin=1; tmax=400; tbar=(tmax+tmin)/2; BB=2(tmax-tmin)/tbar; zm=Log[Rationalize[tmax/tmin]]
gamm[a_, z_]=Gamma[a, 0, z]
Do[J[k, j]=Re[N[gamm[j+1, -k zm]/(-k)^(j+1), 130]], {k, 2, 4}, {j, 0, 2 Nmax+1}]
Do[Do[a[n, j]=J[2, j]/J[2, n+1]; a[n+1, j]=J[4, j]/J[4, n+1], {j, 0, n}]; b[n]=-1; b[n+1]=-1;
  Do[a[m, j]=NSum[J[2, i+j] c[m, i], {i, 0, m+1}, WorkingPrecision->80, NSumTerms->Nmax], {m, 1, n-1}, {j, 0, n}];
  Do[b[m, j]=NSum[J[2, i+n+1] c[m, i], {i, 0, m+1}, WorkingPrecision->80, NSumTerms->Nmax], {m, 1, n-1}];
  Do[a[m, j]=a[m, j]/bb[m], {m, 1, n-1}, {j, 0, n}]; Do[b[m, j]=1, {m, 1, n-1}];
  A=Table[a[i, j], {i, 1, n+1}, {j, 0, n}]; B=Table[b[i, j], {i, 1, n+1}];
  CC=LinearSolve[A, B]; Do[c[n, j]=CC[[j+1]], {j, 0, n}]; c[n, n+1]=1;
  tt[n, z_]=Simplify[Sum[c[n, j] z^j, {j, 0, n+1}]];
  roots=NSolve[tt[n, z]==0, z]; Do[r[n, j]=roots[[j, 1, 2]], {j, 1, n+1}];
  t[n, z_]=Product[(z-r[n, j]), {j, 1, n+1}];
  normgral=NIntegrate[Exp[2z] t[n, z]^2, {z, 0, zm}, WorkingPrecision->50];
  norm[n]=Sqrt[tbar^2 BB/tmin^2/normgral]; t[n, z_]=t[n, z] norm[n], {n, 1, Nmax}];
ROOTS=Table[N[r[n, j], 8], {n, 1, Nmax}, {j, 1, Nmax+1}]; NORM=Table[N[norm[n], 8], {n, 1, Nmax}]

```

Fig. B.1. Mathematica (Wolfram 1991) program to calculate the roots in Eq. (B.12) – they are stored with 8 significant digits in the lower left half of the table ROOTS, and the table NORM contains the normalization coefficients N_n

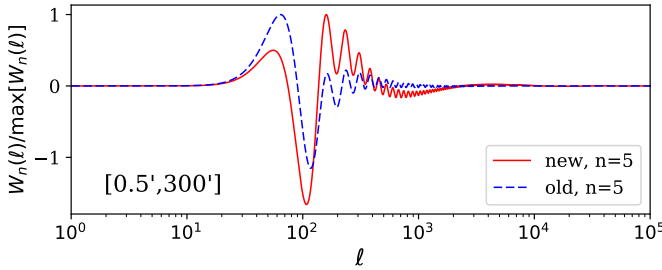


Fig. B.2. Comparison between the new dimensionless (solid red) and the old SEK (dashed blue) COSEBIs. We show the form of the fifth COSEBIs weight function, $W_5(\ell)$. Each curve is normalised with respect to its maximum value. We choose an angular separation interval of 0.5 to 300 arcminutes, to define the weights.

Appendix C: COSEBIs on a sub-interval

In this section we will consider the relation between the COSEBIs on a sub-interval $\vartheta'_{\min} \leq \vartheta \leq \vartheta'_{\max}$, and the original ones on $[\vartheta_{\min}, \vartheta_{\max}]$, where $\vartheta_{\min} \leq \vartheta'_{\min} < \vartheta'_{\max} \leq \vartheta_{\max}$. We denote with B' and ϑ' the relative width and the mean angle inside the subinterval. Furthermore, we denote by $T'_{\pm\mu}(\vartheta)$ the basis functions on the subinterval, which have a support on this sub-interval. The coefficients $\tau'_{\pm\mu}$, defined in analogy with Eqs. (19) and (20), are then obtained from the correlation functions ξ_{\pm} by

$$\tau'_{\pm\mu} = \int_{\vartheta'_{\min}}^{\vartheta'_{\max}} d\vartheta \vartheta T'_{\pm\mu}(\vartheta) \xi_{\pm}(\vartheta) = \sum_{\nu} \mathcal{T}_{\mu\nu}^{\pm} \tau_{\pm\nu}, \quad (\text{C.1})$$

where we used the representation (18) of the correlation function and defined

$$\mathcal{T}_{\mu\nu}^{\pm} = \frac{\bar{\vartheta}^2}{B} \int_{\vartheta'_{\min}}^{\vartheta'_{\max}} d\vartheta \vartheta T'_{\pm\mu}(\vartheta) T_{\pm\nu}(\vartheta). \quad (\text{C.2})$$

Using the relation between the $\tau_{\pm n}$ and the COSEBIs E_n, B_n , we obtain

$$E'_\mu = \frac{\tau'_{+\mu} + \tau'_{-\mu}}{2} = \frac{1}{2} \sum_{\nu} [(\mathcal{T}_{\mu\nu}^{+} + \mathcal{T}_{\mu\nu}^{-}) E_{\nu} + (\mathcal{T}_{\mu\nu}^{+} - \mathcal{T}_{\mu\nu}^{-}) B_{\nu}],$$

$$B'_\mu = \frac{\tau'_{+\mu} - \tau'_{-\mu}}{2} = \frac{1}{2} \sum_{\nu} [(\mathcal{T}_{\mu\nu}^{+} - \mathcal{T}_{\mu\nu}^{-}) E_{\nu} + (\mathcal{T}_{\mu\nu}^{+} + \mathcal{T}_{\mu\nu}^{-}) B_{\nu}].$$

We now look at some properties of the transfer matrices \mathcal{T}^{\pm} . Since the functions T'_{-m} and T_{-n} are related to T'_{+m} and T_{+n}

though the transformation (9), we can apply the Lemma in Sect. 2 and obtain from Eq. (C.2) that

$$\mathcal{T}_{mn}^{-} = \mathcal{T}_{mn}^{+}. \quad (\text{C.3})$$

Furthermore, for $\nu = a, b$, the functions $T_{+\nu}(\vartheta)$ are of the form $x_0 + x_2\vartheta^2$. From the analog of conditions (4) for the $T'_{+\mu}$ functions, we then infer that

$$\mathcal{T}_{ma}^{+} = 0 = \mathcal{T}_{mb}^{+}. \quad (\text{C.4})$$

Similarly, for $\nu = a, b$, the functions $T_{-\nu}(\vartheta)$ are of the form $x_2\vartheta^{-2} + x_4\vartheta^{-4}$, so that the condition (5) yields

$$\mathcal{T}_{ma}^{-} = 0 = \mathcal{T}_{mb}^{-}. \quad (\text{C.5})$$

Together, we then find that

$$E'_m = \sum_{n=1}^{\infty} \mathcal{T}_{mn}^{+} E_n; \quad B'_m = \sum_{n=1}^{\infty} \mathcal{T}_{mn}^{+} B_n. \quad (\text{C.6})$$

This result then shows that the E- and B-mode COSEBIs on the sub-interval can be calculated from the E- and B-mode COSEBIs on the original angular interval. The transfer matrix \mathcal{T}^{+} depends on the choice of basis functions; in general we expect that in order to obtain E'_m to a given accuracy, one needs to use E_n 's up to significantly larger n . However, subdividing the angular interval into sub-intervals, as has been done in some previous work, does not yield any additional information if one chooses the maximum order of COSEBIs properly.

Since in general, \mathcal{T}_{an}^{\pm} and \mathcal{T}_{bn}^{\pm} will be non-zero, the ambiguous modes in the sub-interval will not only depend on the ambiguous modes on the full interval, but some E-/B-modes of the full interval will be transferred to the ambiguous modes on the sub-interval. This is to be expected: the smaller the angular range is, the more pure-mode information gets lost to the ambiguous modes.